DEGREE PROJECT

Feasibility and design of miniaturized Control Moment Gyroscope for a 3-axis stabilized Micro Satellite

Niklas Baker

Space Engineering, masters level
2016

Luleå University of Technology
Department of Computer Science, Electrical and Space Engineering

LULEÅ UNIVERSITY OF TECHNOLOGY

Feasibility and design of miniaturized Control Moment Gyroscope for a 3-axis stabilized Micro Satellite

Niklas Baker

Luleå University of Technology
Dept. of Computer Science, Electrical and Space Engineering
Div. of Space technology

Supervisors
A/P Low Kay Soon
Sheral Crescent Tissera

Examiner
Johnny Ejemalm
Leonard Felicetti

This thesis is presented for the Master of Science in Space Engineering orientation Spacecraft and Instrumentation

October, 2016

Abstract

In this thesis, a feasibility study will be conducted in order to determine if the usage of a control moment gyroscope is a possibility for a micro satellite as its attitude control. The goal is to conclude if gyroscopes are suitable replacements for the current reaction wheels which are acting as the attitude control for the satellite. In the first part of the thesis the general function of the control moment gyroscope and three different types of arrangements are displayed with all their respective advantages and disadvantages. Then one of them will be designed to fit within the restrictions of 1U. The full design of the pyramid configuration was chosen due to its compact size and spherical angular momentum envelope. The full design contains all the components such as motors, flywheels, mounts, frame, screws etc. which provide a cost estimate which is a huge input in determining the feasibility of this thesis. In the future the manufacture of the pyramid configurable control moment gyroscopes shall be tested in the future with a more advanced steering law in order to determine the full potential of the attitude control system.

Preface

I would like to thank my supervisor Associate Professor Low for this great opportunity and interesting thesis.
I would like to thank my supervisor Mihindukulasooriya Sheral Crescent Tissera for his guidance and help whenever needed.
I would also like to thank the staff at the Satellite Research Center at Nanyang Technological University for their hospitality throughout my thesis.
And finally I would like to thank my family to whom I will forever be grateful for all of their encouragement and support throughout my education.

Niklas Baker

Contents

Chapter 1 – Introduction 1
1.1 Introduction . . . 1
1.2 The Satellite . . . 2
1.3 Objectives . . . 3
1.4 Thesis Contribution . . . 3
1.5 Thesis Outline . . . 3

Chapter 2 – Literature Review 5
2.1 Attitude Control System . . . 5
2.1.1 Reaction Wheel . . . 6
2.1.2 Single Gimbal Control Moment Gyroscope . . . 7
2.1.3 Double Gimbal Control Moment Gyroscope . . . 8
2.1.4 Variable Speed Control Moment Gyroscope . . . 8
2.2 Singularity . . . 9
2.3 Mounting Opportunities . . . 10
2.3.1 Cube Configuration . . . 10
2.3.2 Parallel Configuration . . . 12
2.3.3 Pyramid Configuration . . . 14
2.4 Comparison Between Configurations . . . 15
2.4.1 CMG Type . . . 15
2.4.2 Angular Momentum Envelop . . . 16
2.4.3 Choice of Configuration . . . 17
2.5 Mathematical Model . . . 18
2.5.1 Dynamic Rigid Body . . . 18
2.5.2 Dynamic Satellite Model . . . 19
2.5.3 Total Torque of Satellite . . . 20

Chapter 3 – Design 21
3.1 List of Components . . . 22
3.1.1 1U Frame . . . 22
3.1.2 Flywheel Motor . . . 22
3.1.3 Flywheel . . . 23
3.1.4 Gimbal Motor . . . 23
3.1.5 Drive Electronics . . . 25

3.1.6 Slip Ring . . . 25
3.1.7 Connector . . . 25
3.1.8 Reaction Hold . . . 26
3.1.9 Wall . . . 26
3.1.10 Motor and Slip Ring Hold . . . 26
3.1.11 Ball Bearing with Hold . . . 26
3.1.12 Weights . . . 26
3.1.13 Screws . . . 27
3.2 Budget . . . 28
3.3 Final Design . . . 29

Chapter 4 – Technical Specification 31
4.1 Specification List . . . 31
4.1.1 Size . . . 31
4.1.2 Mass . . . 32
4.1.3 Rotation Rate . . . 32
4.1.4 CMG Momentum . . . 32
4.1.5 Interface . . . 33
4.1.6 Operating Temperature Range . . . 33
4.2 Specification Summery . . . 34
4.3 Comparison Between Other CMG . . . 35

Chapter 5 – Conclusion 37
5.1 Conclusion . . . 37
5.2 Future Work . . . 38
5.2.1 Manufacture and Build . . . 38
5.2.2 Air Bed Testing . . . 38
5.2.3 Steering Logic . . . 39
5.2.4 Slip Ring . . . 39
5.2.5 Changing Flywheel Speed . . . 39
5.2.6 Change Configuration . . . 39

Appendix A – MATLAB Code 41
A.1 Angular Momentum Envelope Code . . . 41
1.1.1 Parallel Configuration . . . 41
1.1.2 Pyramid Configuration . . . 42
1.1.3 Cube Configuration . . . 42
1.1.4 Plotting Momentum . . . 43

Appendix B – Angular Momentum Envelope 47

Appendix C – Simulation 53

Appendix D – Datasheets 59

Bibliography **71**

List of Figures

1.1 The 16U Satellite 2
2.1 Reaction Wheel Torque [1] 6
2.2 Single-Gimbal CMG [1] 7
2.3 CMG Singularity 9
2.4 Cube SGCMG Configuration [2] 10
2.5 Mechanical VSDGCMG [3] 12
2.6 Parallel Arrangement VSDGCMG [3] 13
2.7 Pyramid Arrangement [4] 14
2.8 Pyramid Singularity 16
3.1 Exploded View of SGCMG Unit 21
3.2 1U Frame 22
3.3 The Flywheel developed by NTU 23
3.4 Reaction Unit 24
3.5 Display of Cenrtre of Mass of Reaction Mount 27
3.6 The different type of screws 27
3.7 Different Views of the Pyramid Arrangement 29
4.1 Pyramid Clearance 31
4.2 Difference Types of CMG 35
B.1 Parallel Envelope Full Axis 47
B.2 Parallel Envelope X-Y Axis 48
B.3 Parallel Envelope X-Z Axis 48
B.4 Pyramid Envelope Full Axis 49
B.5 Pyramid Envelope X-Y Axis 49
B.6 Pyramid Envelope X-Z Axis 50
B.7 Cube Envelope Full Axis 50
B.8 Cube Envelope X-Y Axis 51
B.9 Cube Envelope X-Z Axis 51
C.1 Combined display of the gimbal angle, gimbal rate and torque 54
C.2 Sun Pointing Error 55
C.3 Displaying each of the gimbal Angle 56
C.4 Displaying each of the gimbal rate 57
C.5 Displaying each of the torque 58

List of Tables

1.1 Satellite Sizes [5] 1
1.2 16U Satellite info 2
2.1 Advantages and Disadvantages of various types of CMG as compared to RW [6, 7] 15
2.2 Comparisons of Configurations and Momentum Envelopes 16
3.1 Trade-off Gimbal Motors 24
3.2 Budget of one SGCMG Unit 28
3.3 Mass Budget 28
3.4 Cost Budget 28
4.1 Technical Specification 34
4.2 CMG Comparison 35

CHAPTER 1

Introduction

1.1 Introduction

The usage of Control Moment Gyroscopes (CMG) as an Attitude Control System (ACS) is nothing new in the space industry. In the past they have been used in large spacecraft such as Skylab and the International Space Station (ISS) but they were expensive and extremely hard to manufacture. In the past 20 years or so, there has been a great leap in the creation of cheap Commercial-off-the-shelf (COTS) components which enable us to use CMG on small satellites [8–10].

Table 1.1: Satellite Sizes [5]

Group Name	Wet Mass	
Large Satellite	$>$ 1000 kg	Medium-Large Satellite
Medium Satellite	500-1000 kg	
Mini Satellite	100-500 kg	Small Satellite
Micro Satellite	10-100 kg	
Nano Satellite	1-10 kg	
Pico Satellite	$<$1 kg	

The main reason why CMG is so attractive to use on smaller satellites is they have a high torque amplification. They can generate much greater torque with less energy when compared to ordinary reaction wheels (RW) which are normally used in smaller satellites.

CMG make the satellite more agile, increases its slew rate, increases the efficiency of the remote sensing and decreasing the total mass of the satellite. Also the CMG usually has less mass than RW and with higher torque that can be produced the less power is needed for small attitude adjustments [5, 11].

1.2 The Satellite

The Satellite Research Centre(SRC) at NTU in Singapore has in the past year shown interest in developing a micro satellite. The company Innovative Solution In Space [12] offers a satellite which has a 4U base and then there are four levels stacked on top of each other creating a 16U satellite. The satellite will be equipped with four stacks of solar cells which is the same size as a side of a satellite shown in Figure 1.1.

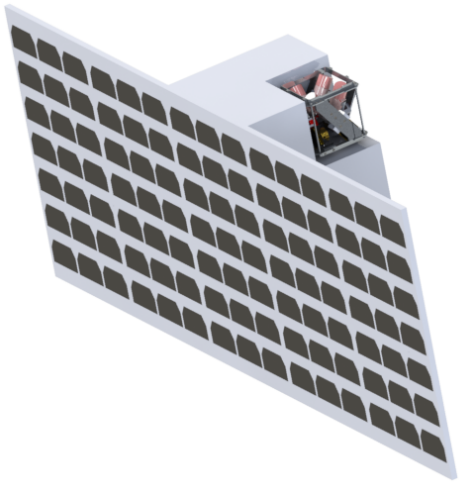

Figure 1.1: The 16U Satellite

Table 1.2: 16U Satellite info

- 226.3 x 226.3 x 454 mm
- Average U mass 2 kg
- Solar cell mass 1.5 kg
- Total General Mass 38 kg

The rotation of the satellite is determined by its moment of inertia which is centred around the center of mass. In the top corner of the satellites body the CMG design is shown and in the calculation it has the same mass as an average U.

$$J = \begin{bmatrix} I_{xx} & I_{yy} & I_{zz} \end{bmatrix} = \begin{bmatrix} 0.6826 & 0.2731 & 0.6862 \end{bmatrix} kgm^2 \tag{1.1}$$

Currently SRC has only used reaction wheels for the satellites which they have launched but no micro satellites have been launched. With the increase of satellite size and mass SRC is considering CMGs as an alternative to RWs for the ACS. This implementation of the CMGs hardware should prove to be more efficient in manoeuvring this satellite with such higher inertia then for nano satellite used by SRC in the past.

In this thesis a proposal of a CMG system shall be put forward to determine if this change in attitude control is feasible.

1.3 Objectives

In this thesis there are three main objectives,

- Perform a feasibility study on the design and implementation of a CMG for a 3-axis stabilized agile micro satellite that can perform slew maneuvers of 3 deg/s.
- Use Computer Aided Design(CAD) to design CMG to fit within an envelope of less then 1U as per CubeSat standard 1U has the dimension $91.6 \times 91.6 \times 95.8$ mm [13] and a mass lower than 2 kg.
- Provide a specification list that displays the limits of the CMGs.

1.4 Thesis Contribution

Providing an alternative to RWs that will provide enhanced performance while using less energy. Present a full design and list of components that will achieve the set goals. Ways of communication and ability to control the alignment of the satellite.

1.5 Thesis Outline

Chapter 2: The general information of different CMGs and different configurations are displayed. Chapter 3: The design aspect, the different components and the final assembly are presented. Chapter 4: The design specifications are listed and displayed in a table. Chapter 5: The conclusion of this thesis and what can be done in the future and what improvements can be made.

CHAPTER 2

Literature Review

2.1 Attitude Control System

There are two types of attitude control on a spacecraft, passive and active control. Both of which utilize Newton's laws of inertia, action and reaction which state the following,

"If a body is not subject to any net external force, it either remains at rest or continues in uniform motion" and

"When two particles interact, the force on one particle is equal and opposite to the force on the other" [14].

With passive attitude control, the satellites dynamics are utilized in order to control its attitude, such as spin stabilized-, gravity gradient torque control etc. In the active control category there are different types of actuators, momentum exchange devices, thrusters, magnetic torques that control the spacecraft. Each one of these actuators requires a command in order to maneuver the satellite thus saying that it is under active control [10, 15].

The reason why momentum exchange devices are so suited for spacecraft is that they only require electricity to work so they will have the same characteristics throughout the mission. The momentum devices are able to produce more torque than magnetic torques and momentum devices are independent of the magnetic field which are vital to the function of the magnetic torques [16]. This is a clear advantage compared to a thruster which needs fuel to work, where the mass of the fuel will decrease under the duration of the mission. Which must be taken into consideration because this will alter the total inertia of satellite [17].

However, a satellite cannot be equipped with only one set of momentum exchange devices because they have a limit of how much momentum they can store. At some point during a mission the satellite is almost certain to experience a disturbance in one direction over a long period of time. This results in the momentum devices will be unable to produce any more torque. For example, when a reaction wheel can no longer increase its speed. Then the satellite will need to use other actuators in SRC case, magnetic

torques [18] to perform a so called momentum dumping. This action will allow the momentum exchange devices to reduce the momentum stored which enables them to produce more torque [10, 15, 16].

2.1.1 Reaction Wheel

The Reaction Wheel(RW), shown in Figure 2.1, is the most basic form of a momentum exchange device which is often used in satellites in order to control its attitude. A RW is made up of two main components, a motor and a wheel, both of which correlate to the angular momentum that a RW can produce according to equation 2.1, the angular momentum of a rotational movement [19],

$$h_{RW} = I_{wheel}\omega_{wheel} \tag{2.1}$$

where I_{wheel} is the inertia of the wheel and ω_{wheel} is how fast the motor is rotating the wheel. The torque T is shown in the figure below and is referred to in the rest of the thesis as τ. The change of the angular momentum is always aligned with the angular momentum. For this reason a satellite is usually equipped with a cluster four RW to achieve full 3 degree of freedom(DOF), one for each axis and an extra for redundancy [16].

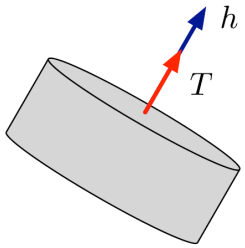

Figure 2.1: Reaction Wheel Torque [1]

To control the spacecraft the RWs will change their rotational speed ω_{motor} to change the angular momentum and torque.This ensures that the vectors will always point towards the same direction, without experiencing any singularities (see section 2.2).

There are two ways to increase the torque output that a RW can develop. One option is by increase the inertia of the wheel that is rotating. The other option is to invest in a more powerful motor that can achieve a higher rotational speed. Both of the two alternatives will cost mass and money while increasing the energy consumption of the RW [1].

2.1.2 Single Gimbal Control Moment Gyroscope

The most basic CMG is the Single-Gimbal Control Moment Gyroscope(SGCMG), but it is still more complex than an ordinary RW. An ordinary SGCMG consists of a RW that will spin at a constant speed and what sets it apart from a RW is that instead of changing its speed, the motor is able to rotate instead. The RW is rotated around it gimbal axis δ, as shown in Figure 2.2.

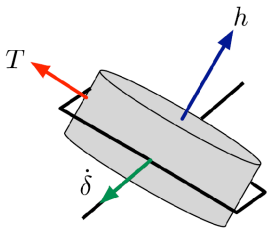

Figure 2.2: Single-Gimbal CMG [1]

The reason why CMG are so attractive to use in small spacecraft is because of the way a CMG produces its torque, as shown in equation 2.2 below [6, 11],

$$\tau = h \times \dot{\delta} \tag{2.2}$$

where h is the angular momentum of the RW, $\dot{\delta}$ is the gimble rate (how fast it rotates around its gimbal axis) and τ is the torque produced. With the RW rotating with a constant speed, constant h, the torque is controlled only by the gimbal rate. This gives the CMG a greater torque magnification, which allows for a large amount of torque be produced with a small amount of energy because it requires less energy to rotate the RW around its gimbal axis than to change the speed of the flywheel.

The torque vector that the SGCMG produces will always be perpendicular to the angular momentum and gimbal axis. This means that the torque vector will not be pointing at the same direction all the time. The vector will rotate at the same speed as the gimbal rate [10, 11]. It is the main cause why the CMG are much more complicated to control compared to RW. The CMG requires a more sophisticated steering algorithm that takes into consideration the change in torque and more importantly the angular momentum.

2.1.3 Double Gimbal Control Moment Gyroscope

The Double Gimbal Control Moment Gyroscope(DGCMG) is similar to a SGCMG, except that it has one extra DOF providing one more gimbal axis, allowing it to produce torque in two directions instead of one. The extra gimbal axis is placed alongside the torque vector, as shown in Figure 2.2.

With the extra gimbal axis the complexity and cost is increased compared to a SGCMG. Also the torque vectors are dependent upon the two gimbal axis, meaning if the two gimbal planes are not parallel they cannot produce its highest possible torque in one direction.

For the DGCMG to operate normally, it requires more hardware, gears etc.and more complicated software in order to avoid the singularity zones. It is also imperative to keep the two gimbal axis separated from each other to avoid the gimbal lock(when the two torque vectors are aligned with each other). If a gimbal lock occurs the DGCMG cannot produce any torque in two directions and it will act like a SGCMG, thus defeating the point of installing a DGCMG [10, 20].

The largest DGCMG ever created for space application are on the ISS. This cluster of parallel configuration can produce a maximum torque of $300Nm$ [7, 9].

2.1.4 Variable Speed Control Moment Gyroscope

This is the most complex CMG because you combine the variable speed control moment gyroscope(VSCMG) with a SGCMG or a DGCMG. The VSCMG enables one to control the rotational speed of the RW in a CMG. By controlling the speed of the RW the CMG will have one more DOF. However while containing one extra DOF to control, this axis will not experience the same torque amplification. As this axis will be controlled as a RW instead of rotation around a gimbal axis. This CMG configuration requires the largest amount of energy to operate and with the highest abundance of parts in its construction. There are more components susceptible to damage or fatigue thus reducing the reliability of the CMG [21].

2.2 Singularity

The major disadvantage of the CMG is what is called singularity, that is when the CMG cannot produce any torque at all to its designated axis.

Lets say for an instance a CMG is mounted to produce torque along the x-axis. In its initial position the CMG will have its torque vector aligned with the x-axis, as shown in Figure 2.3a, in a certain moment a gimbal rate is applied to the CMG which will make the torque vector rotate in the same speed as the gimbal rate. After a duration the torque vector will be perpendicular to the x-axis, as shown in Figure 2.3b, at this moment the CMG will not produce any any torque along the x-axis. This is what results in a singularity [10, 22].

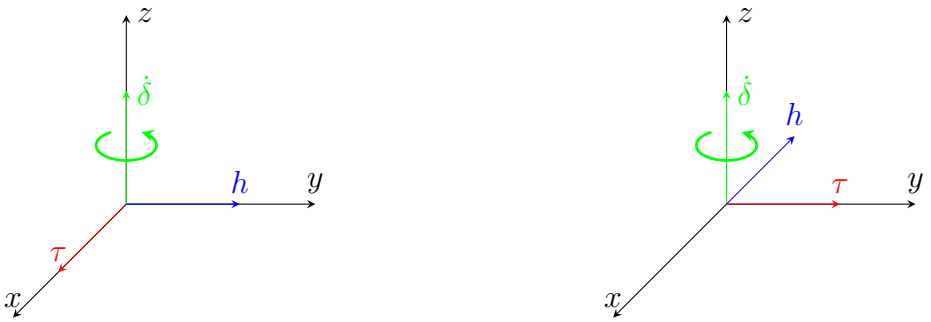

(a) Before Rotation (b) After Rotation

Figure 2.3: CMG Singularity

There are both software and hardware solutions that can be applied in order to avoid this singularity. The hardware method is to physically limit the rotational movement of the gimbal angle so it cannot rotate 90^o, which could create more problems than it would solve. A much simpler and cheaper way to solve this problem though software, in which a steering logic is applied to avoid the singularity zones [11].

2.3 Mounting Opportunities

While the mounting of ACS can be arranged differently, they all have the same goal, to ensure that torque can be applied to all of the axis of the satellite. The following states three examples of how a cluster of CMGs can be arranged to achieve full control on all axis.

2.3.1 Cube Configuration

In this configuration there are two SGCMGs for each axis that will only produce torque on one axis. At the beginning the two RWs are aligned on one axis, rotating in opposite directions, producing two angular momentum vectors in both positive and negative directions according to the so called "right hand rule". This is called the scissor approach where the gimbals are rotating in opposite directions. The torque vector produced by rotating the RWs, does not point in the same direction all the time. It will rotate with the same velocity as $\dot{\delta}$ shown in equation 2.2 and that will produce a torque on an unwanted axis. To counteract this the two RWs will rotate in different directions around their respective gimbal vectors. The unwanted torques from the two CMGs will cancel each other out and will only produce torque in one direction.

With a cluster of 6 SGCMGs with two SGCMGs for each axis, as shown in Figure 2.4, this configuration will manage to produce torque on all axis [2].

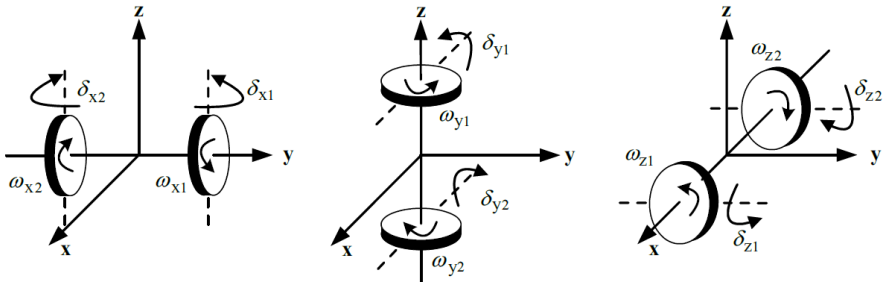

Figure 2.4: Cube SGCMG Configuration [2]

The figure above explain the expression of the angular momentum vector for this arrangement, eq 2.3-2.6. The figure shows the RWs at their original position, $\delta = 0$, while rotating their respective angular momentum created from eq 2.1 around their gimbal axis.

$$h_x = \begin{bmatrix} -h_{x1} \sin \delta_{x1} + h_{x2} \sin \delta_{x2} \\ h_{x1} \cos \delta_{x1} - h_{x2} \cos \delta_{x2} \\ 0 \end{bmatrix} \tag{2.3}$$

$$h_y = \begin{bmatrix} 0 \\ -h_{y1}\sin\delta_{y1} + h_{y2}\sin\delta_{y2} \\ h_{y1}\cos\delta_{y1} - h_{y2}\cos\delta_{y2} \end{bmatrix} \tag{2.4}$$

$$h_z = \begin{bmatrix} h_{z1}\cos\delta_{z1} - h_{z2}\cos\delta_{z2} \\ 0 \\ -h_{z1}\sin\delta_{z1} + h_{z2}\sin\delta_{z2} \end{bmatrix} \tag{2.5}$$

The total angular momentum vector for this configuration is the combination of eq: 2.3, 2.4 and 2.5

$$\mathbf{h} = \begin{bmatrix} -h_{x1}\sin\delta_{x1} + h_{x2}\sin\delta_{x2} + h_{z1}\cos\delta_{z1} - h_{z2}\cos\delta_{z2} \\ h_{x1}\cos\delta_{x1} - h_{x2}\cos\delta_{x2} - h_{y1}\sin\delta_{y1} + h_{y2}\sin\delta_{y2} \\ h_{y1}\cos\delta_{y1} - h_{y2}\cos\delta_{y2} - h_{z1}\sin\delta_{z1} + h_{z2}\sin\delta_{z2} \end{bmatrix} \tag{2.6}$$

2.3.2 Parallel Configuration

With this configuration an equal number of DGCMG are placed parallel to each other. Using the scissor approach here the RWs and gimbals will rotate in opposite directions. In this case, shown in Figure 2.5 [3], it consists of two RWs that can produce torque with its two gimbal rotation around two axis. In order to produce torque in the final axis the RWs is able to change its speed, making this configuration a variable-speed double gimbal CMG(VSDGCMG) [3]. This technique can be found on ISS to control its attitude. However ISS uses four VSDGCMG instead of two [9].

This configuration does not control all of its axis with the gimbal approach. Two out of the three axis of the satellite are controlled by the gimbals while the last axis is controlled by a RWs that can change its speed. This axis does not have the same torque amplification as the other two axis and requires more energy to control.

This configuration is mechanically complicated, with an extra gimbal motor and gears required in this system. When you introduce gears in any system you will need to remove all the gear backlash that occurs. This drastically decreases the precision of the gimbal axis. This problem can be solved by adding some anti-backlash gears [2].

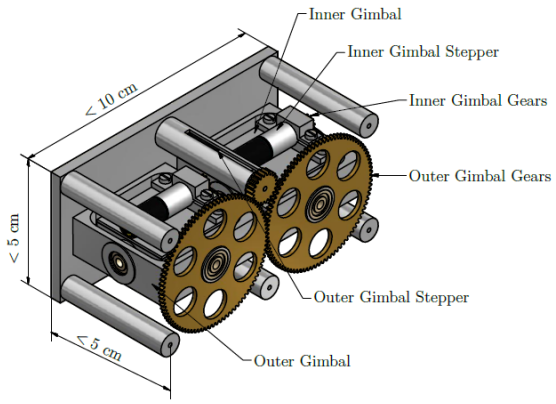

Figure 2.5: Mechanical VSDGCMG [3]

The angular momentum matrix for the this configuration is derived from Figure 2.6 as in the previous arrangement.

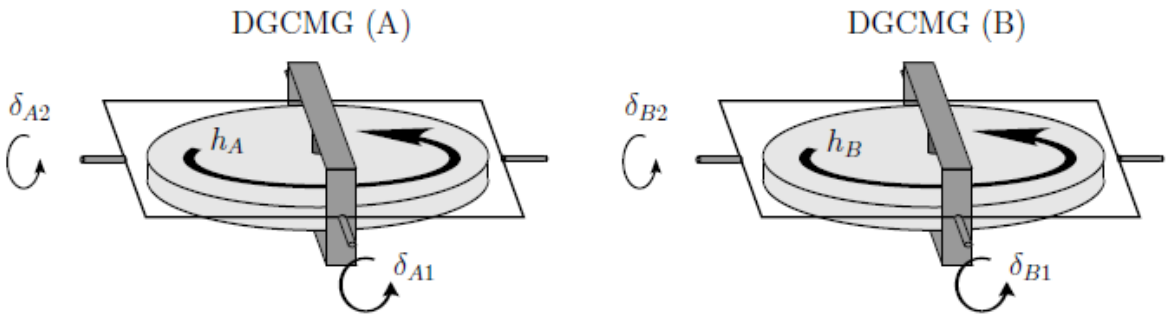

Figure 2.6: Parallel Arrangement VSDGCMG [3]

$$\mathbf{h} = \begin{bmatrix} -h_A \cos\delta_{A1} \sin\delta_{A2} - h_B \cos\delta_{B1} \sin\delta_{B2} \\ h_A \sin\delta_{A1} + h_B \sin\delta_{B1} \\ h_A \cos\delta_{A1} \cos\delta_{A2} + h_B \cos\delta_{B1} \cos\delta_{B2} \end{bmatrix} \tag{2.7}$$

The angular momentum matrix can be simplified by setting the angles to rotate in opposite directions and substituting the angular momentums h_A and h_B to display the change in angular momentum,Δh, that is controlled by changing the rotational speed of the RWs.

$$\delta_{A1} = -\delta_{B1} = \delta_1, \delta_{A2} = -\delta_{B2} = \delta_2 \tag{2.8a}$$

$$h_A = h_0 + \frac{1}{2}\Delta h \tag{2.8b}$$

$$h_B = -h_0 + \frac{1}{2}\Delta h \tag{2.8c}$$

With this simplification shows the simplified angular momentum matrix of the parallel configuration, which is dependent on $[\delta_1 \ \delta_2 \ \Delta h]^T$

$$\mathbf{h} = \begin{bmatrix} -2\cos\delta_1 \sin\delta_2 h_0 \\ 2\sin\delta_1 h_0 \\ \cos\delta_1 \cos\delta_2 \Delta h \end{bmatrix} \tag{2.9}$$

2.3.3 Pyramid Configuration

One of the most common mounting configurations of SGCMGs is the pyramid approach. This configuration is appealing because it is able to achieve full 3 DOF control with the least amount of SGCMG. A cluster of no more than four CMGs are needed for full control of a satellite. The CMGs are placed on the same plane with to ensure their respective angular momentum vectors will originally be aligned to the same plane. Their respective gimbal axis tilted with a certain skew angle β. By tilting the gimbal axis this enables all the CMGs to create torque that affects all three axis, this is shown in Figure 2.7. The skew angle β is usually set to 54.74^o because this angle will provide the most optimal spherical momentum envelope capability with the smallest area of singularity zones [4, 11, 23].

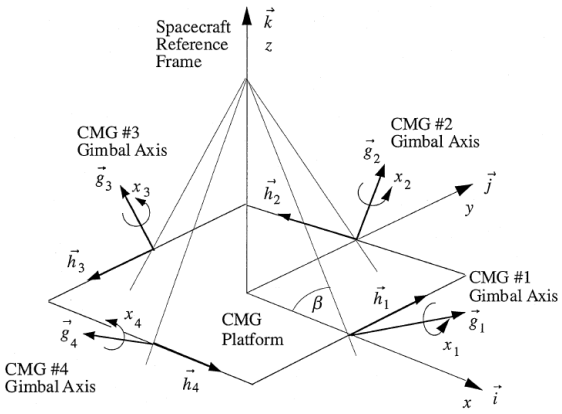

Figure 2.7: Pyramid Arrangement [4]

The angular momentum matrix for the pyramid configuration is equation 2.10.

$$\mathbf{h} = h_0 \begin{bmatrix} -\cos\beta\sin x_1 - \cos x_2 + \cos\beta\sin x_3 + \cos x_4 \\ \cos x_1 - \cos\beta\sin x_2 - \cos x_3 + \cos\beta\sin x_4 \\ \sin\beta\sin x_1 + \sin\beta\sin x_2 + \sin\beta\sin x_3 + \sin\beta\sin x_4 \end{bmatrix} \tag{2.10}$$

2.4 Comparison Between Configurations

Several factors are taken into consideration in choosing the appropriate configuration for the satellite.

2.4.1 CMG Type

There is a difference between the output torque of a SGCMG and DGCMG. The two CMGs create torque in a similar manner. However the DGCMG is able to generate torque upon two axis. It does not have the same capability in one axis as compared to the SGCMG because the total torque output on one axis is dependent on two gimbal axis for the DGCMG while for the SGCMG it is only dependent on one. This means if the one of the the DGCMG gimbal axis is not zeroed the output torque will be smaller as compared to the SGCMG.

As mentioned before, with an extra DOF the DGCMG becomes more difficult to manufacture due to complexity and cost. Furthermore if a VSCMG is added to the system this is one extra functional component that must be managed by the CMG.

During the operation of the satellite, all the components will deteriorate which eventually leads to reliability issues. When the VSCMG is combined with a SGCMG or DGCMG, one extra DOF to the CMG will be added. However the extra DOF will not have the same torque amplification as the other axis because essentially you treat that axis as a RW, which increases the energy consumption of the system.

Table 2.1: Advantages and Disadvantages of various types of CMG as compared to RW [6, 7]

CMG Type	Advantage	Disadvantage
SGCMG	Better Torque Magnification	Singularity States
DGCMG	Torque Magnification Extra Degree of Freedom	Cost and Size Mechanical Complex
VSCMG	Extra Degree of Freedom	Reliability Power

2.4.2 Angular Momentum Envelop

The angular momentum that the three CMG configurations can produce is displayed in Appendix B. The values displayed in Table 2.2 are taken from there.

Table 2.2: Comparisons of Configurations and Momentum Envelopes

Configuration	Number of CMG	Max Momentum	Momentum per CMG
Parallel	2	2 h_0	1 h_0
Pyramid	4	3.2662 h_0	0.8166 h_0
Cube	6	4 h_0	0.6667 h_0

The angular momentum envelop developed by the Cube and Parallel configurations have similar characteristics. This simplifies the steering laws as the surface of the envelope lacks any surface singularities.

However with the pyramid configuration the steering law needs to be slightly more complicated in order to control the spacecraft. Figure 2.8 shows the momentum envelop of the pyramid configuration. The red arrows indicate the singularity zones that the configuration experiences. There are eight zones in total, four shown in the figure and the other four are located at the same position but on the negative z-axis side. If the SGCMG are angled such that the angular momentum enters one of these singularities zones, the efficiency will decrease harshly. For this reason an advanced steering law is needed in order to make sure that the singularity zones will be avoided, which is the cheapest option.

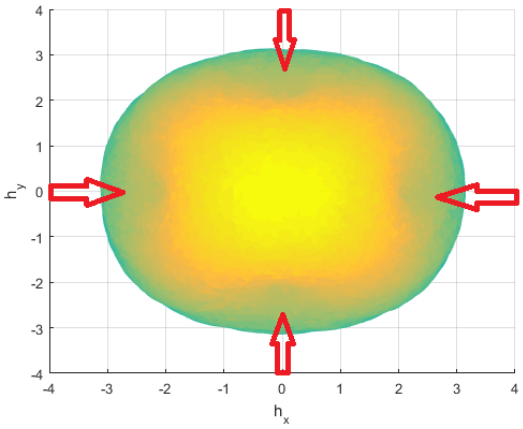

Figure 2.8: Pyramid Singularity

2.4.3 Choice of Configuration

The choice of configuration that will be designed, simulated and used will be the pyramid configuration due to the following reasons :

- Number of Motors
  Because the size of the CMG cluster is an important issue the pyramid configuration is more suited than the cube configuration.

- Design Simplicity
  It is imperative to make the design as simple as possible, if the parallel configuration was chosen it would add much more design complexity and a vital loss of the gimbal torque from one axis. The variable speed RW of the parallel configuration uses more power then the pyramid configuration.

- The Momentum Envelop
  The envelop for the pyramid is greater than the parallel arrangement. Even though the cube configuration envelope is larger then the pyramid it does not compensate for the complexity and difference in physical size. The singularity problem of the pyramid can be compensated with the steering law.

- Reliability and Cost
  The pyramid configuration has fewer components compared to the other two arrangements. With the minimum amount of component, this will increase the reliability of the system, less components to break. The pyramid configuration also have the least amount of motors, which will drastically reduce the cost as the motors will be the most expensive part in the CMG.

2.5 Mathematical Model

To describe the rotation of a body there are two aspects that one needs to consider,the attitude kinematics and the attitude dynamics of the body. With the kinematics you look analyse the body without consideration the force of the torques the body may experience and with looking at the dynamics you do.

2.5.1 Dynamic Rigid Body

The body of a satellite can be seen as a rigid body. It will not experience any deformations, so to get a mathematical model of the satellite we need to take a look at the basic equation for angular momentum and this is defined in equation 2.11 [19] below

$$\mathbf{H} = \mathbf{I}\boldsymbol{\omega} \tag{2.11}$$

where $\mathbf{I}$ is the object's, body's, mass moment of inertia, $\boldsymbol{\omega}$ is the object's angular velocity.

To represent when the body start to rotate along its internal reference frame i, is the derivative of equation 2.11

$$\frac{d}{dt}^{i}\mathbf{H} = \left(\frac{d}{dt}^{i}\mathbf{I}\right)\boldsymbol{\omega} + \mathbf{I}\left(\frac{d}{dt}^{i}\boldsymbol{\omega}\right) \tag{2.12}$$

rewriting it so the equation is representing the moment in the body frame

$$\mathbf{M} = \frac{d}{dt}^{i}\mathbf{H} = \mathbf{I}_b\dot{\boldsymbol{\omega}}_b + \boldsymbol{\omega}_b \times \mathbf{I}_b\boldsymbol{\omega}_b \tag{2.13}$$

The total angular momentum that the satellite will experience $\mathbf{H}_{net}$, according to Newton's law of action and reaction, will be the amount of angular momentum of the satellite and the angular momentum produced by the actuators on board the spacecraft.

$$\mathbf{H}_{net} = \mathbf{h}_{body} + \mathbf{h}_{act} \tag{2.14}$$

where h is the angular momentum, by knowing that $\mathbf{h}_{body}$ can be represented by equation 2.11, substitution equation 2.14 in to equation 2.13

$$\mathbf{M} = \mathbf{I}_{body}\dot{\boldsymbol{\omega}}_{body} + \dot{\mathbf{h}}_{act} + \boldsymbol{\omega}_{body} \times (\mathbf{I}_{body}\boldsymbol{\omega}_{body} + \mathbf{h}_{act}) \tag{2.15}$$

This is the general mathematical motion of a rotating satellite, all equation and reasoning above is from [10, 15, 24, 25].

2.5.2 Dynamic Satellite Model

From equation 2.15 with the correct actuators CMG and on the correct body a satellite. $\mathbf{M}$ is the external torque $\mathbf{N}_{ext}$ that acts on the satellite.

$$\mathbf{I}_s\dot{\boldsymbol{\omega}}_s + \dot{\mathbf{h}}_{CMG} + \boldsymbol{\omega}_s \times (\mathbf{I}_s\boldsymbol{\omega}_s + \mathbf{h}_{CMG}) = \mathbf{N}_{ext} \tag{2.16}$$

The internal control torque $\mathbf{u}$ generated by the CMGs is the following

$$\dot{\mathbf{h}}_{CMG} + \boldsymbol{\omega}_s \times \mathbf{h}_{CMG} = -\mathbf{u} \tag{2.17}$$

where equation 2.17 into 2.16 and assumes that the satellite does not experience any external torques.

$$\mathbf{I}_s\dot{\boldsymbol{\omega}}_s + \dot{\boldsymbol{\omega}}_s \times \mathbf{I}_s\boldsymbol{\omega}_s = \mathbf{u} \tag{2.18}$$

The control input can now be described as

$$\dot{\mathbf{h}}_{CMG} = -\mathbf{u} - \boldsymbol{\omega}_s \times \mathbf{h}_{CMG} \tag{2.19}$$

and rewritten as

$$\dot{\mathbf{h}}_{CMG} = \mathbf{A}(\delta)\dot{\boldsymbol{\delta}}_{gimbal} \tag{2.20}$$

where $\mathbf{A}(\delta) = \frac{\partial \mathbf{h}}{\partial \delta}$ is the Jacobian matrix of the cluster of angular momentum of the CMGs and $\dot{\boldsymbol{\delta}}_{gimbal}$ is the angular gimbal velocity which can be described as following

$$\dot{\boldsymbol{\delta}}_{gimbal} = \mathbf{A}^T(\mathbf{A}\mathbf{A}^T)^{-1}\dot{\mathbf{h}}_{CMG} \tag{2.21}$$

all the equations above from [10, 15, 24].

The Jacobian of the pyramid configuration is displayed in the equation below.

$$\mathbf{A}(\delta)_{Py} = h_0 \begin{bmatrix} -\cos\beta\cos\delta_1 & \sin\delta_2 & \cos\beta\cos\delta_3 & -\sin\delta_4 \\ -\sin\delta_1 & -\cos\beta\cos\delta_2 & \sin\delta_3 & \cos\beta\cos\delta_4 \\ \sin\beta\cos\delta_1 & \sin\beta\cos\delta_2 & \sin\beta\cos\delta_3 & \sin\beta\cos\delta_4 \end{bmatrix} \tag{2.22}$$

The equations above show how changing the rotation of the gimbal rate correlates with the control of the satellite.

The implementation of this steering law is shown in Appendix D.

2.5.3 Total Torque of Satellite

To achieve the high slew rate of $3^o/s$ of a rest-to-rest motion the CMGs need to provide sufficient torque to counteract the satellite torque. The following calculation represent the 16U satellite housing maneuver where the satellite will rotate 180 degree to achieve the desired slew rate. This action will take 60 seconds.

The equation to calculate the torque of a rotating body is as follow:

$$\sum \tau = I\ddot{\theta} = I\alpha \tag{2.23}$$

where I is inertia of the satellite which is set to $I = 0.84kgm^2$, the value from equation 1.1 with an extra safety margin around 20% and α is the acceleration of the satellite. For our case we can make the assumption that during the housing maneuver the satellite acceleration will be constant. The equation of constant acceleration is presented below [19].

$$\theta = \theta_0 + \omega_0 t + \frac{1}{2}\alpha t^2 \tag{2.24}$$

During the housing maneuver which is a rest-to-rest motion. The satellite will start from rest position, accelerate to half way, then decelerate the satellite to a rest position pointing in the desired direction. This is done by rotating the CMGs in one direction around their gimbal axis. When the satellite has travelled 90^0 the CMGs will rotate in the opposite direction. The maximum angular speed the satellite will achieve can be determined by

$$\omega = \omega_0 = \alpha t \tag{2.25}$$

The following values are used in the equations above are $\theta = 90^o$, $t = 30s$ and $\theta_0 = \omega_0 = 0$, equation from [5, 19, 22, 26].

Which gives the following values $\alpha = 0.2005^o/s^2 = 0.0035rad/s^s$, $\omega_{max} = 5.9989^o/s = 0.1047rad/s$, $\tau = 2.9mNm$.

This means that the satellite body will experience a torque of $2.9mNm$ in order to rotate 180^o.

CHAPTER 3

Design

The design presented in this thesis will take the already existing RWs that are planned to be used in SRC's next 16U satellite. The difference is that torque will be achieved by rotating the motor around a gimbal axis instead of increasing the speed of the reaction wheel. The four identical CMG units will make up the pyramid configuration. Figure 3.1 displays an exploded view of one CMG unit.

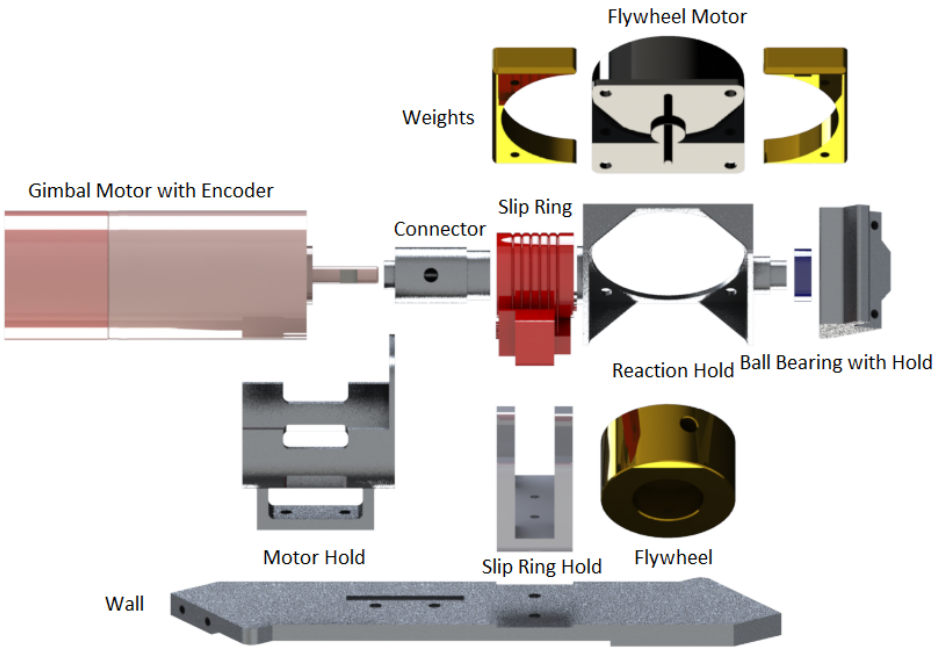

Figure 3.1: Exploded View of SGCMG Unit

3.1 List of Components

In this section the components in the exploded view in Figure 3.1 will be listed and discussed, as will the reasoning of the design and why the components are used in the CMG unit.

3.1.1 1U Frame

The component shown in Figure 3.2 is the frame that the pyramid configuration will be mounted in. The standard frame can be purchased from Innovative Solutions In Space [12]. The frame in the figure however is modified so that the four CMGs units will mounted within. This frame will be mounted on the satellite structure with its 8 frame holders. This restricts the CMGs to the outer dimensions of the frame which measures $91.6 \times 91.6 \times 95.8mm$. The frame is modified in order to hold the four CMGs while still being able to be mounted onto the satellite structure. These modifications include relocating holes for the ball-bearing holdings and the repositioning of the frame holdings. The overall mass of one standard 1U cubesat lays around 100 grams.

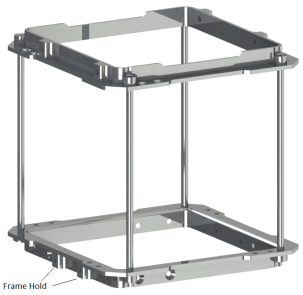

Figure 3.2: 1U Frame

3.1.2 Flywheel Motor

The flat DC motors come from the company Faulhaber and is named Series 2610012B SC. These motors have been used in prior satellites with success and are already available at SRC. The dc motor was chosen is because it has a ample speed range, reliability, small size and dynamic response [27]. This motor is suited for satellites because the motor is compact and it comes with an integrated speed controller. The motor is controlled with pulse width modulation(PWM) command. Throughout the motors operational lifetime it will rotate with a constant angular velocity of $\omega_{fm} = 5000RPM$, a high velocity while not exceeding the optimal capability of the motor.

3.1.3 Flywheel

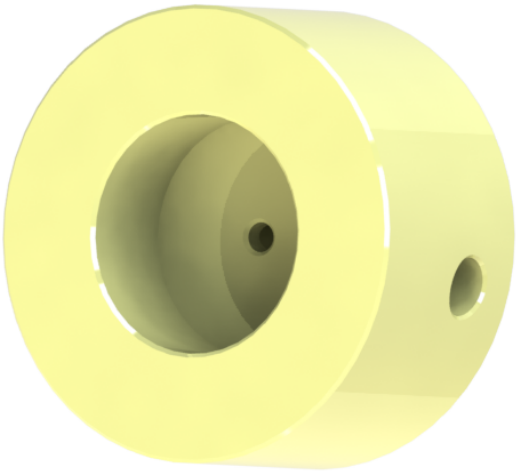

Figure 3.3: The Flywheel developed by NTU

The flywheel that will be used for the configuration will be a flywheel developed by NTU shown in Figure 3.3

This brass flywheel has a diameter of $23mm$ and a height of $12mm$ and a mass of $35.22g$. The moment of inertia of the flywheel is $I_{fw} = 2636.40gmm^2$.

This flywheel will be rotating at a constant speed while in operation and will produce constant angular momentum. Using equation 2.1 with the values of I_{fw},ω_{fm} the angular momentum of each one of the reaction wheels will be able to develop an angular momentum of $h_0 = 1.4mNm^{-s}$. With the pyramid mounting the four CMG, $3.2662h_0$ will be produced according to the findings in Table 2.2.

The maximum angular momentum that this pyramid configuration can achieve is $h_{max} = 4.5 * 10^{-3}kgm/s^2$.

3.1.4 Gimbal Motor

The function of the gimbal motor is to rotate the reaction units around their respective gimbal axis are either a stepper motor or a DC motor, the dc motor is preferred. The same company, Faulhaber, will be used for this selection of the dc motor.

The amount of power required for the motor is dependent on the moment of inertia of the reaction unit displayed in Figure 3.4. One reaction unit has the inertia of $I_{ru} = 3667gmm^2$ and the torque required to rotate it is the time derivative of equation 2.1.

$$\tau = I_{ru}(\frac{\omega_f - \omega_s}{t}) \tag{3.1}$$

The maximum torque occurs when the gimbal motor goes from the most negative speed to its most positive speed. For this calculation the inertia is set to $I_{ru} = 4000gmm^2$. This gives a safety margin of 9%. The angular velocity, ω, is the range from $-100RPM$ to $+100RPM$ at time, $t = 10ms$. The motor requires a torque of $8.4mNm$.

During the operational lifetime the gimbal motors need to provide a constant feedback of information while being able to control the position and speed. This requires an encoder in order to provide the sufficient information. Faulhaber only offers encoders

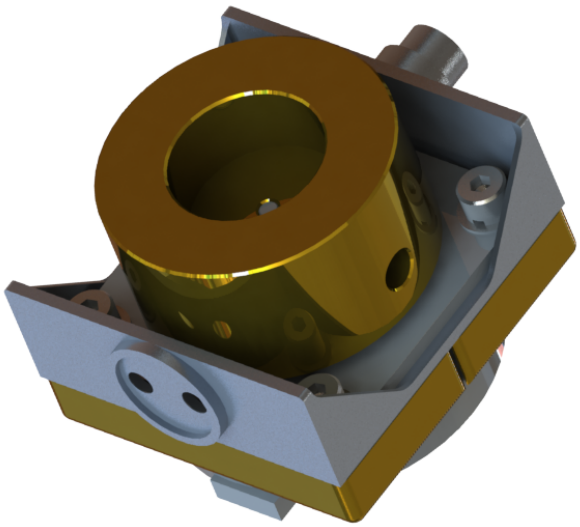

Figure 3.4: Reaction Unit

together with the DC motors, so a stepper motor cannot be used. The type of encoder that is needed is an absolute encoder, which provides unique angular values for each position of the motor shaft. This is required in order to compensate for the disturbance during the launch of the satellite. The violence of the satellite launch will almost certainly disturb the alignment of the CMGs. The angular momentum will be drastically reduced if this misalignment is not corrected.

Faulhaber offers two brushless DC motors that meet the requirements above and can be fitted within the size constraints of the 1U frame. The two motors are from the BX4/BX4 S from the 2232 series, both of which have the option of being equipped with an absolute encoder. The Table 3.1 below displays a trade-off between the two.

Table 3.1: Trade-off Gimbal Motors

	BX4 S	BX4	
Torque	8.5	18	mNm
Power	19	23	W
Stall Torque	27.8	58.7	mNm
Mass	64	65	g
Rotor Inertia	4.2	5.1	gcm^2
Ang. Acc.	66	115	$*10^3 rad/s^2$

With these considerations taken into account, the more powerful motor, BX4, is se-

lected. The full name of the gimbal motor is Series 2232012BX4 AES-4096. The absolute encoder has 4096 lines per revolution, which has the capability to measure steps as small as 0.0879^o.

3.1.5 Drive Electronics

To control the gimbal motor a set of drive electronics is required. The drive electronics need to be compatible with the motor and the encoder, which is the MCBL 3002 P AES, which will be ordered together with the gimbal motor. The flywheel motor has its own drive electronics integrated so there is no need for an external drive. The gimbal drive electronics are relatively large (see Appendix D). Due to their size and the restrictions of the 1U frame, the drive electronics will not be mounted inside the 1U together with the rest of the CMG. The location of the drive electronics will be together with the rest of the electrical components on-board the satellite.

3.1.6 Slip Ring

The reaction unit will be rotated many times around its axis. In order to control the flywheel motor, it needs to be connected with six cables. To avoid entanglement the wires require a connection from rotationary to stationary. This is done with the LPS-06, a separate slip ring from JINPAT electronics. This slip ring consists of two parts, stationary and rotating, which are more compact than a commonly used combined slip ring. It has the 6 circuits model required for the flywheel motors. The advantage of this model is that it will contribute minimal disturbances, such as electrical noise, to the complete system [28]. The slip ring will limit the rotational speed of the gimbal motor. The maximum operational speed of the slip ring is limited 100 RPM. Higher speed may result in loss of connection to the reaction motor.

The slip ring will be the component that will have the shortest life span. With its operational life of more than 50 000 000 rotations, which result in a total life span of the CMG being approximately one year.

3.1.7 Connector

The connector will ensure that the reaction unit will always be connected to the motor shaft, slip ring and reaction hold. There is a groove in the motor shaft of the gimbal motor where a flat head screw will hold the connector in place. The outer diameter of the connector has the same diameter as the slip ring which will ensure that they will rotate at the same velocity. The smaller end of the connector be resting on the ball bearing equipped on the motor. The reaction hold will be mounted on the other end of the connector. This fitted within the slot on the reaction hold to guarantee they will stay connected during disturbances.

3.1.8 Reaction Hold

At one end, the reaction hold will be connected with the connector and will be fastened with two screws to ensure full response when being rotated. At the other end, the holding will have its shaft inserted in the ball bearing to ensure smoother rotation with less friction therefore less fatigue. The reaction hold will also hold the weights and flywheel motor. They will be held together with four screws with washers to reduce wear the tear. The tops of the screwheads will be mounted on the motor side and the weights on the bottom have threaded holes that will hold everything together.

3.1.9 Wall

The wall will hold the CMGs in place while staying connected to the frame of the 1U. As shown in Figure 3.2 the top and bottom frames are held together with four beams. The distance between each of the beams differs such that the wall is designed with the shortest distance between the beams. The wall will provide the desired skew angle of $54.74deg$, therefore giving the pyramid a near spherical momentum envelope.

3.1.10 Motor and Slip Ring Hold

These two holds will align the motor and slip ring, making the rotation for all the components as smooth as possible. These two components will be fastened to the wall with $M2$ screws. To ensure a permanent location, the wall which they will be mounted to is fitted with grooves where the two holdings will be mounted. The purpose of these groves is to reduce the shaking the CMG will experience during launch.

3.1.11 Ball Bearing with Hold

The ball bearing hold will hold the reaction unit in place, giving it the extra support when it rotates. Within the hold, a ball bearing will be fitted on which the reaction hold will rest. The ball bearing which is from MISUMI [29] cost $SGD5.57$ and has an inner radius of $5mm$ outer radius of $9mm$ and thickness of $3mm$. This determines the main dimension of the reaction hold, which is design to fit on the bottom frame.

3.1.12 Weights

In order to achieve the smooth rotation of the reaction unit, the unit should rotate around its centre of mass. Originally with only the flywheel mounted on the motor, the center of mass was located high up because the flywheel mass is greater than the motor. Without any modifications, rotating the reaction unit around the high central of mass the volume requirement for the CMGs would overextend the 1U dimensions requirements. Therefore the central of mass need to be lowered in order to reduce the volume of the CMGs when

they are rotating. To lower the centre of mass, brass weights are now mounted beneath the reaction hold. Figure 3.5 shows the difference in the centre of mass, which is portrayed as the black and white circle. Without the weights, the distance between the centre of mass and rotational center is $2mm$. With the weights equipped on the reaction hold, the distance is reduced to $0.06mm$, which decreases the distance by 97%.

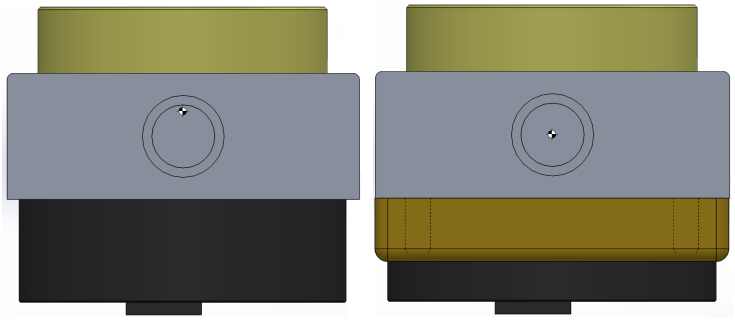

(a) Without Weights (b) With Weights

Figure 3.5: Display of Cenrtre of Mass of Reaction Mount

3.1.13 Screws

It is useful to use the same type of screw for all the holes in throughout the design in order to simplify the construction of CMGs. In the design there are four different types of screws. All the screws are from the company MISUMI [29] which provides a good search history and CAD deign for download. Four SCBS2-6 which are head cap screws with washer set which will hold the reaction unit together. Two SFB3-12 which will hold the slip ring to its hold with flat head cap. SSHH-316L-M3-3 which is a socket set screw, will connect the connector to the motor shaft of the gimbal motor and for the rest of the holes, eighteen flat head caps called SFB2-4 are required.

Figure 3.6 displays the different types of screws, with the socket set screw at the top, followed by the flat head cap screw and the socket head cap with washers at the bottom.

Figure 3.6: The different type of screws

3.2 Budget

Table 3.2: Budget of one SGCMG Unit

Table 3.3: Mass Budget

Unit	Mass,g
Gimbal Motor with Encoder	65
Wall (S)	16.88
Motor Hold (S)	6.12
Connector (S)	2.73
Slip Ring	~ 4
Slip Ring Hold (S)	6.01
Reaction Mounting (S)	2.72
Flywheel (S)	36.628
Flywheel Motor	20.1
Weights($2x$) (S)	5.65
Ball Bearing with Hold (S)	7.31
Screws (S)	5.43
Drive Electronics	7
Total	185.578

Table 3.4: Cost Budget

Unit	Cost,SGD
Gimbal Motor with Encoder	276
Wall	M
Motor Hold	M
Connector	M
Slip Ring	60
Slip Ring Hold	M
Reaction Mounting	M
Flywheel	M
Flywheel Motor	M
Weights($2x$)	M
Ball Bearing with Hold	5.57+M
Screws	15.07
Drive Electronics	615
Total	$971.587 + M$

With the exeption of weights and screws, the (S) in Table
3.3 are items that are designed with SOLIDWORKS and they are made of aluminium which has the density of $2700kg/m^3$. The weights and screws are made from brass and stainless steel which have the density of $8500kg/m^3$ and $\rho = 7700kg/m^3$ respectively. The cost for a single SGCMG unit is in Table 3.4, M stands for manufacturing. The cost fort manufacturing is determined by the manufacturer that will manufacture the components made with the CAD software. For the full pyramid configuration, four CMG units are required together with the frame. According to [12], the price for 1U structure is SGD 3227.88, which derives the full price of the pyramid arrangement as SGD $7114 + M$.

3.3 Final Design

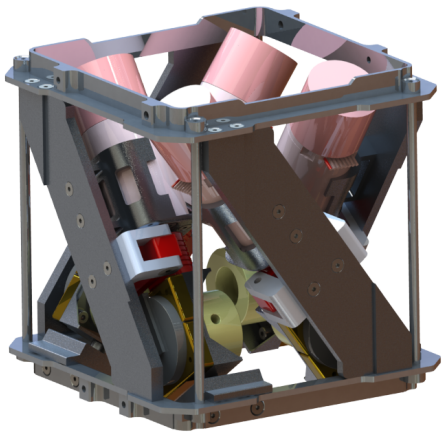

(a) Full Pyramid Configuration

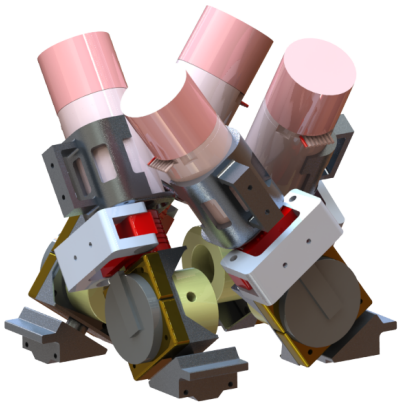

(b) Without Frame and Wall

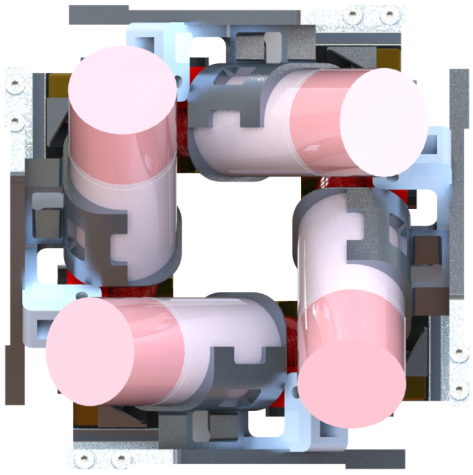

(c) Top View

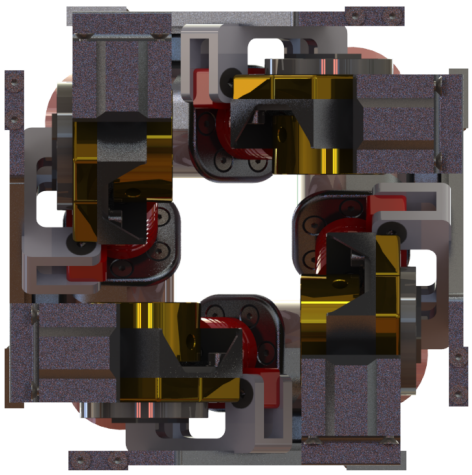

(d) Bottom View

Figure 3.7: Different Views of the Pyramid Arrangement

CHAPTER 4

Technical Specification

4.1 Specification List

4.1.1 Size

The size of the CMG, which determines the scale of the reaction unit, is mainly dependent on the size of the gimbal motor and the flywheel. The reaction unit for this configuration is able to rotate $360deg$ without colliding with the other reaction units and the frame. In Figure 4.1 the reaction unit is rotated $360deg$ to display the clearance. The length of one

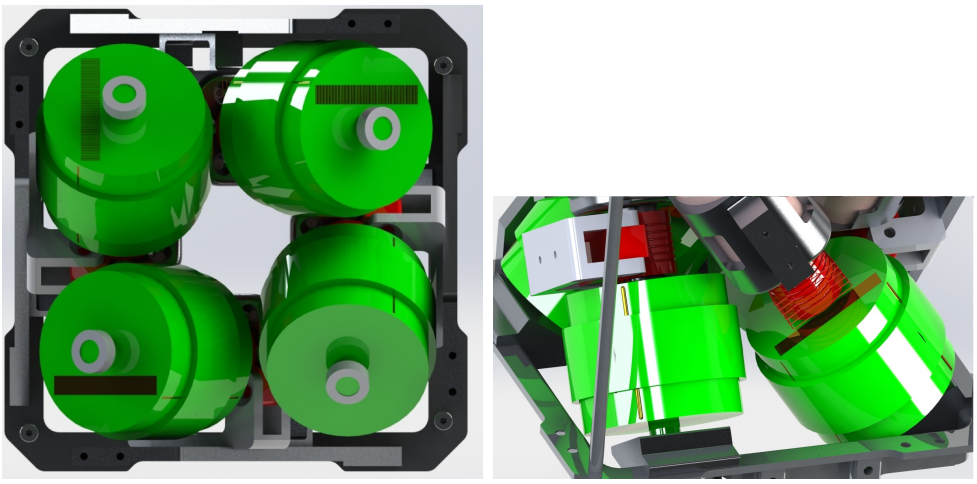

(a) Displaying the rotation clearance (b) Displaying frame clearance

Figure 4.1: Pyramid Clearance

CMG unit is $114.66mm$, which exceeds the 1U restriction whether the unit is mounted vertically or horizontally. However the design has a skew angle of $54.74deg$, which allows for this length of the CMG.

4.1.2 Mass

As stated in Table 3.3 the mass of one CMG unit is lower than $200g$. The pyramid configuration requires a total of four CMG units to operate. The four CMG will be mounted inside the modified 1U frame. The primary structure mass of the frame is under than $100g$ [12]. Hence, the total mass of the complete CMG arrangement is below than $842.312g$, which is almost half of the mass requirement stated in the thesis objective.

4.1.3 Rotation Rate

There are eight dc motors in total in the pyramid arrangement. The flywheel motor will rotate at a constant speed in order to conserve energy. The rotational speed that these motor will generate is $5000RPM$ in the same direction. The gimbal motor, however is rated to go much faster, it is limited to the range of -100 to $+100RPM$ to increase the lifetime of the CMGs. The speed resolution is controlled by the 16-bit controller with a pulse width module. This gives the gimbal motor a resolution of $0.1022RPM$ and the flywheel motor a resolution of $0.0946RPM$.

4.1.4 CMG Momentum

The angular momentum for one CMG unit is dependent on how fast the flywheel rotates. With the inertia displayed in Section 3.1.3 it will rotate at a speed of $5000RPM$. This gives one CMG unit an angular momentum of $h_0 = 1.4mNm^{-s}$.

The total angular momentum that the pyramid arrangement provides is an almost perfect sphere as shown in Appendix B. With that being said, there is a slight difference of 3.5% in the angular momentum along the axis. The x and y axis develop the same amount of angular momentum and the z direction will have this extra 3.5% of momentum. The angular momentum is therefore $(3.152 \times 3.152 \times 3.2262)h_0mNm^{-s}$

4.1.5 Interface

Six cabals are required to control one flywheel motor. Four of these cables are for basic needs such as ground, power and output signal for the speed control. The other two cables control the motor, one to control its direction and the other is PWM controlled to determine its speed.

The gimbal motors are controlled by the additional motion controller incorporated in the drive electronics. The motion controller interface is either RS232 or CAN. With this motion controller there are several functions that determine the motors speed of the motors. The two main motion controllers functions that are of interest for this usage are the position and velocity control functions. With both of these functions the characteristics of the acceleration can be manipulated. All of these functions are provided in the communication manual from Faulhaber [30].

4.1.6 Operating Temperature Range

The operation temperature of the CMG is dependent on therman tolerance of the plastic and electrical components since all of the structure and some of the mountings are made from aluminium, which are not as temperature dependent. The list below shows the temperature range of the critical components.

1U Frame -40 to $+80^o$

Flywheel Motor -25 to $+80^o$

Slip Ring -20 to $+60^o$

Gimbal Motor -40 to $+100^o$

Encoder -40 to $+100^o$

Motion Controller -25 to $+85^o$

Where the 1U information is taken from [12] and the remaining list is from the datasheet in Appendix D.

From the list above it is clear that the slip ring determines the operational temperature range hence this slip ring have the worst temperature tolerance.

4.2 Specification Summery

Table 4.1: Technical Specification

Specification	Data
Size	
Single CMG	$45.22 \times 33.11 \times 114.65mm$
Pyramid Array	$95.8 \times 95.8 \times 95.8mm$
Mass	
One CMG Unit	$185.578g$
Pyramid Array	$842.312g$
CMG Momentum	
Single CMG	$1.4mNm^{-s}$
Pyramid Array	$4.413 \times 4.413 \times 4.573mNm^{-s}$
Rotation Rate	
Flywheel Motor	$5000RPM$
Gimbal Motor	$\pm 100RPM$
Interface	RS232 or CAN Flywheel Motor Speed Control Gimbal Motor Speed & Position Control
Operation Temperature Range	-20 to $+60^o$

4.3 Comparison Between Other CMG

In this section the thesis CMG will be compared with three other CMG units displayed in 4.2, two from other thesis and one CMG, Honeybee, which is commercially sold.

Table 4.2: CMG Comparison

Information	Thesis CMG	Honeybee	SwampSat	PhD Lappas
Mass(g)	842.312	600	$<$500	$\sim$ 1000
Size(mm^3)				
Array	879 212	2 263 200	-	-
Skew Angle(deg)	54.74	-	40	54.73
Momentum/Mass (g/mNm^{-s})				
Single	0.007 54	0.343	-	0.000 35
Array(max)	0.005 43	0.343	-	0.001 05
Flywheel Speed (RPM)	5000	8000	8000	11 200
Operation Temperature Range (Deg)	-20 to $+60$	-20 to $+85$	-40 to $+80$	0 to $+70$
Arrangement	Pyramid	Scissor	Pyramid	Pyramid
Satellite	Micro	Small	Nano	Micro

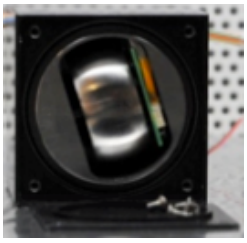

(a) CMG from Honeybee Robotics [31]

(b) CMG of SwampSat [20]

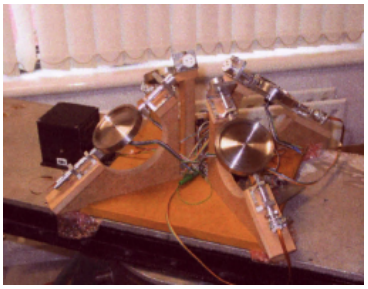

(c) CMG of V.Lappas [5]

Figure 4.2: Difference Types of CMG

CHAPTER 5

Conclusion

5.1 Conclusion

The CMG in this thesis compares well with the CMG developed by Lappas. The angular momentum and its envelope are much greater and it will have a lower mass as well. Its operational temperature range is greater which results in less energy required in order to maintain the internal temperature of the satellite. This CMG is able to generate a much higher angular momentum because of the higher inertia of the flywheel. Even though the thesis flywheel speed is lower, the inertia of the flywheel makes up for the difference in magnitude.

There are not that many comparisons that can be made with the SwampSat CMG because there are no specific numbers for the momentum mentioned in that specific thesis. However the difference in the skew angle is due to the size restriction of the satellite. The SwampSat is a 3U Nano satellite which allocated an allowance of half U for its CMG configuration. The SwampSat's lower skew angle provides an envelope that will not be spherical as in this thesis. If there is no need for such a high momentum envelope, using a smaller skew angle is a great way of reducing the size of the CMG.

When it comes to the commercially sold CMG from Honeybee there are no comparisons to prove that they are able to out perform the design presented in this thesis. This is because the angular momentum of the CMGs, which result in a difference in size of the satellites which the CMG from Honeybee are able to control. The CMG from Honeybee is able to control a lager satellite with a maximum mass of $500kg$, which is more than ten times greater than the 16U satellite presented in this report. The CMG from Honeybee is more than double the size of the thesis CMGs. The size restriction will determine the decision to buy the CMG from Honeybee or to continue developing this pyramid configured CMG arrangement presented in this thesis. This is dependent on several factors such as what is the mission of the satellite, other instruments on board and the total mass of the satellite.

The CMG presented in this thesis will be able to control a 16U satellite within the size

restriction of 1U. The mass of the CMG is more than half of its maximum mass which leaves room for developing a greater angular momentum in the future.

To answer the question of the main title of this thesis, yes, it is feasible to develop an attitude control system consisting of CMGs to adjust the pointing in three axis of a micro satellite. Whether or not the CMG will outperform a standard reaction wheel set up in both torque and consuming less energy which will allow in lesser usage of momentum dumping maneuvers which will happen if the CMGs are able to generate more torque as well as providing a much greater slew rate of the satellite.

5.2 Future Work

The future work for this project can be derived into two parts, one part is to manufacture and test the design and the second part is to provide improvements to the design in order to increase the performance of the CMG.

5.2.1 Manufacture and Build

The next step is to contact a manufacturing company to manufacture all the components developed using the CAD software, followed by building the whole CMG inside the modified 1U. It begins with completing each of the SGCMG units then fit them inside the frames and mount the four CMGs to the respective walls and bearing holds which are then mounted on to the frame.

5.2.2 Air Bed Testing

With the CMGs assembled in the pyramid configuration, testing on the attitude control system can be done in order to determine the output torque and the energy consumption of the system. This is done with an air test bed where compressed air is pushing a table up from underneath. With only air holding up the table, the table will essentially experience no friction. With the attitude control system mounted upon the bed, together with some other mass to give the same inertia as the 16U satellite, the test bed can then be rotated around one axis to determine the performance of the system.

5.2.3 Steering Logic

The implementation of a sophisticated steering logic will increase the efficiency of the CMG. A good steering logic will avoid the singularity zones which results in decreasing the overall gimbal rates of the system. There is no need to increase the rate to compensate for the lack of angular momentum in the singularity zones. There are many types of steering laws displayed in the References list. These shows different applications of logic that will improve the steering law. A working steering law which results in lower gimbal rate will increase the lifetime of the CMGs since they do not need to rotate at higher speeds.

5.2.4 Slip Ring

The weakest part of the CMG unit can arguably be the slip ring. It is the component that will have the shortest lifetime due to the rotating reaction hold and it has the narrowest temperature range of the components. Changing this component may result in a longer lifetime and a wider temperature range which can be more suitable for the satellite. However if a new slip ring is selected there may be some changes to the design of the CMG.

5.2.5 Changing Flywheel Speed

There are two configurations that can be applied to improve the CMGs in term of the rotational speed on the system. One option is to increase the flywheel speed when the torque vector of the CMGs enters the singularity zones, operating the flywheel motor as a VSCMG. Increasing the speed when entering the singularity zones would increase the angular momentum and compensate for the lack of momentum thus providing a more spherical momentum envelope. The other option is just to increase the constant speed of the flywheel. This will generate a higher angular momentum envelope and thus increase the overall torque. Because it will just spin in a higher velocity, the only extra energy required is the energy for the acceleration to the higher speed. When the flywheel reaches a higher velocity it will consume the same amount of electricity as before but will shorten the operational lifetime of the CMG.

5.2.6 Change Configuration

Throughout the literature review I came across a tetrahedra mounting configuration that would slightly increase the angular momentum envelope. The reason why this configuration is not displayed in this thesis is because the size requirement for this configuration would not fit within the 1U dimension. To implement the tetrahedra configuration would require smaller motors. Looking beyond Faulhaber for the selection of motors would be an option to solve this problem.

APPENDIX A

MATLAB Code

A.1 Angular Momentum Envelope Code

1.1.1 Parallel Configuration

```
h_0 =1;
start = 0;
step = 30; % 1,20,36
stop = 360;
range = stop - start;
VelocityStart = -2*h_0;
VelocityStop = 2*h_0;
VelocityStep = (abs(VelocityStart)+abs(VelocityStop))/(range/step);
h_pa_store = [];
parallelcount = 1;
for a1 = start : step : stop
    for b1 = start : step : stop
        for a2 = start : step : stop
            for b2 = start : step : stop
                for VelocityChange  = VelocityStart : VelocityStep : VelocityStop
                h_a = h_0 + (0.5*VelocityChange);
                h_b = -h_0+ (0.5*VelocityChange);
                A = [a1 b1 VelocityChange a2 b2];
                hx =-h_a*cos(a1)*sin(a2)-h_b*cos(b1)*sin(b2);
                hy = h_a*sin(a1) + h_b*sin(b1);
                hz = h_a*cos(a1)*cos(a2)+h_b*cos(b1)*cos(b2);
                h_pa_store(:,parallelcount) = [hx; hy ;hz];
                parallelcount = parallelcount +1;
                end
            end
        end
    end
```

```
    filename = strcat('C:\Users\Samsung\Dropbox\Master Thesis\Matlab\ParallelEnvelop\test\
    %filename = strcat('saving folder location', num2str(a1)); desctiption of above
    save(filename,'h_pa_store')
    parallelcount=1;
    clc;
end
```

1.1.2 Pyramid Configuration

```
beta = degtorad(54.74); %The optimal gimbal angle
h_0 = 4.1888e-05;
step = 30
start = 0;
stop = 360;
range = stop - start;
pyramidcount = 1;
info = 1;
for cmgfour = start : step : stop
    for cmgthree = start : step : stop
        for cmgtwo = start : step : stop
            for cmgone = start : step : stop
                A = [cmgfour cmgthree cmgtwo cmgone];
                hx =-cos(beta)*sin(cmgone)-cos(cmgtwo) ...
                    +cos(beta)*sin(cmgthree)+cos(cmgfour);
                hy = cos(cmgone)-cos(beta)*sin(cmgtwo) ...
                    -cos(cmgthree)+cos(beta)*sin(cmgfour);
                hz = sin(beta)*sin(cmgone)+sin(beta)*sin(cmgtwo)...
                    +sin(beta)*sin(cmgthree)+sin(beta)*sin(cmgfour);
                h_py = h_0 * [hx; hy ;hz];
                h_py_store(:,pyramidcount) = h_py * 10^-3;
                pyramidcount = pyramidcount+1;
            end
        end
    end
    filename = strcat('C:\Users\Samsung\Dropbox\Master Thesis\Matlab\PyramidEnvelop\test\h
%filename = strcat('saving folder location', num2str(cmgfour)); desctiption of above
    save(filename,'h_py_store')
    pyramidcount=1;
    clc;
end
```

1.1.3 Cube Configuration

```
h_0 = 1;
step = 30;
start = 0;
stop = 360;
```

```
range = stop - start;
h_sc_store = zeros(3,((range/step)+1)^5);
h_sc_store_1 = [];
cubecount=1;
for dz1 = start : step : stop;
    for dz2 = start : step : stop;
        for dy1 = start : step : stop;
            for dy2 = start : step : stop;
                for dx1 = start : step : stop;
                    for dx2 = start : step : stop;
                        A = [dz1 dz2 dy1 dy2 dx1 dx2];
                        hx = -sind(dx1) + sind(dx2) + cosd(dz1) - cosd(dz2);
                        hy =  cosd(dx1) - cosd(dx2) - sind(dy1) + sind(dy2);
                        hz =  cosd(dy1) - cosd(dy2) - sind(dz1) + sind(dz2) ;
                        h_sc = h_0 * [hx; hy ;hz];
                        h_sc_store(:,cubecount)= h_sc;
                        cubecount = cubecount+1;
                    end
                end
            end
        end
    end
    filename = strcat('C:\Users\Samsung\Dropbox\Master Thesis\Matlab\CubeEnvelop\step
    %filename = strcat('saving folder location', num2str(dz1)); desctiption of above
    save(filename,'h_sc_store')
    cubecount=1;
    clc;
end
```

1.1.4 Plotting Momentum

```
step =30;
start = 0;
stop = 360;
A = [];
h_sc_store_Post = [];
h_py_store_Post = [];
h_pa_store_Post = [];
for dz1 = start : step : stop; % Cube Configuration
    % Select where to load the angular momentum on you computer
    filename = strcat('C:\Users\Samsung\Dropbox\Master Thesis\Matlab\CubeEnvelop\step
    A = load(filename);
    h_sc_store_Post = [h_sc_store_Post A.h_sc_store];
end
cubemax = sqrt((h_sc_store_Post(1,:)).^2 + (h_sc_store_Post(2,:)).^2 + (h_sc_store_Po
maximum_cube = max(cubemax)
figure(1) % Plot with dots
view(155,20)
```

```
hold on
view(155,20)
xlabel('h_x')
ylabel('h_y')
zlabel('h_z')
set(gca,'xlim',[-5 5],'ylim',[-5 5],'zlim', [-5 5])
set(get(gca,'ZLabel'),'Rotation',0)
shading interp
plot3(h_sc_store_Post(1,:),h_sc_store_Post(2,:),h_sc_store_Post(3,:),'b.');
figure(2) %Sufrace plot
view(155,20)
xlabel('h_x')
ylabel('h_y')
zlabel('h_z')
set(gca,'xlim',[-5 5],'ylim',[-5 5],'zlim', [-5 5])
set(get(gca,'ZLabel'),'Rotation',0)
shading interp
h_sc = h_sc_store_Post';
k = boundary(h_sc);
hold on
trisurf(k,h_sc(:,1),h_sc(:,2),h_sc(:,3),'EdgeColor','none')
for dz1 = start : step : stop;  %Pyramid Configuration
    % Select where to store the angular momentum on you computer
    filename = strcat('C:\Users\Samsung\Dropbox\Master Thesis\Matlab\PyramidEnvelop\test\h
    A = load(filename);
    h_py_store_Post = [h_py_store_Post A.h_py_store];

end
pyramidmax = sqrt((h_py_store_Post(1,:)).^2 + (h_py_store_Post(2,:)).^2 + (h_py_store_Post
figure(2)
view(155,20)
plot3(h_py_store_Post(1,:),h_py_store_Post(2,:),h_py_store_Post(3,:),'b.');
figure(4)
view(155,20)
title('Angular Momentum Pyramid')
xlabel('h_x')
ylabel('h_y')
zlabel('h_z')
grid on
set(gca,'xlim',[-4 4],'ylim',[-4 4],'zlim', [-4 4])
set(get(gca,'ZLabel'),'Rotation',0)
shading interp
h_py = h_py_store_Post';
l = boundary(h_py);
hold on
trisurf(l,h_py(:,1),h_py(:,2),h_py(:,3),'EdgeColor','none')
for dz1 = start : step : stop; %Parallel
    % Select where to store the angular momentum on you computer
    filename = strcat('C:\Users\Samsung\Dropbox\Master Thesis\Matlab\ParallelEnvelop\test\
    A = load(filename);
```

```
    h_pa_store_Post = [h_pa_store_Post A.h_pa_store];

end
paramidmax = sqrt((h_pa_store_Post(1,:)).^2 + (h_pa_store_Post(2,:)).^2 + (h_pa_store
maximum_parallel = max(paramidmax)
figure(3)
view(155,20)
plot3(h_pa_store_Post(1,:),h_pa_store_Post(2,:),h_pa_store_Post(3,:),'b.');
figure(6)
view(155,20)
title('Angular Momentum Parallel')
xlabel('h_x')
ylabel('h_y')
zlabel('h_z')
grid on
h_pa = h_pa_store_Post';
j = boundary(h_pa);
hold on
trisurf(j,h_pa(:,1),h_pa(:,2),h_pa(:,3),'EdgeColor','none')
```

Appendix B

Angular Momentum Envelope

Displays more of the angular momentum envelope of the three mounting configuration discussed in section 2.3 produced by the MATLAB code in Appendix A.1. It was mentioned in the thesis that the gimbal angle may be restricted in some way, however with these envelops all the gimbal will rotate 360 degrees all independent to each other and the variable speed for the parallel configuration is with the range is from $-2h_0$ to $2h_0$.

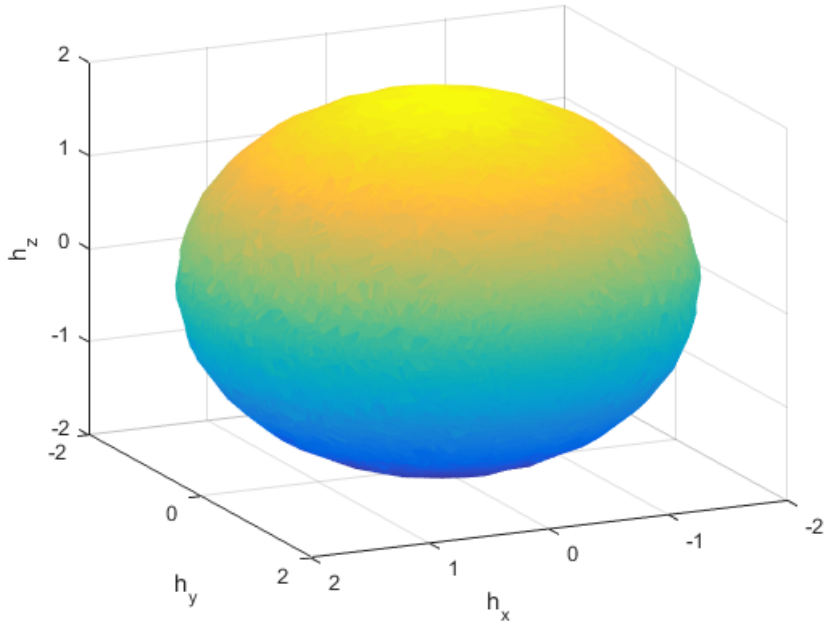

Figure B.1: Parallel Envelope Full Axis

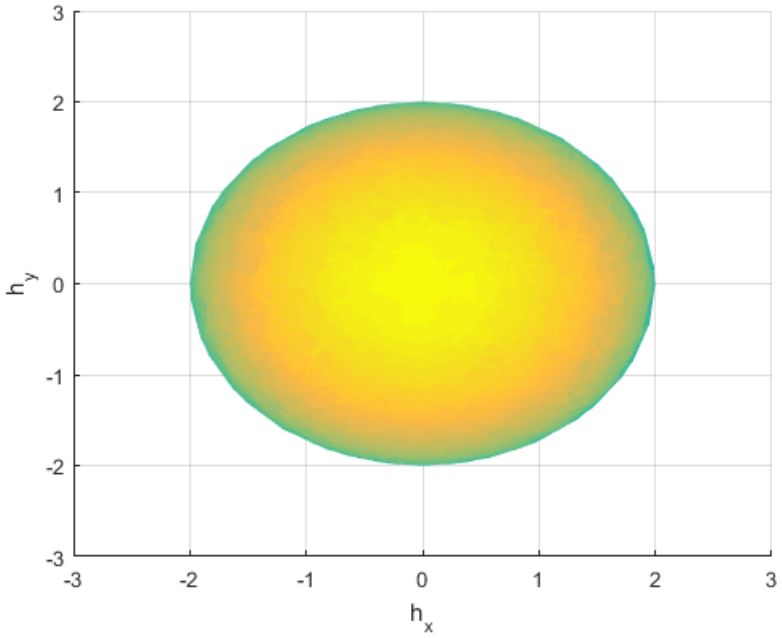

Figure B.2: Parallel Envelope X-Y Axis

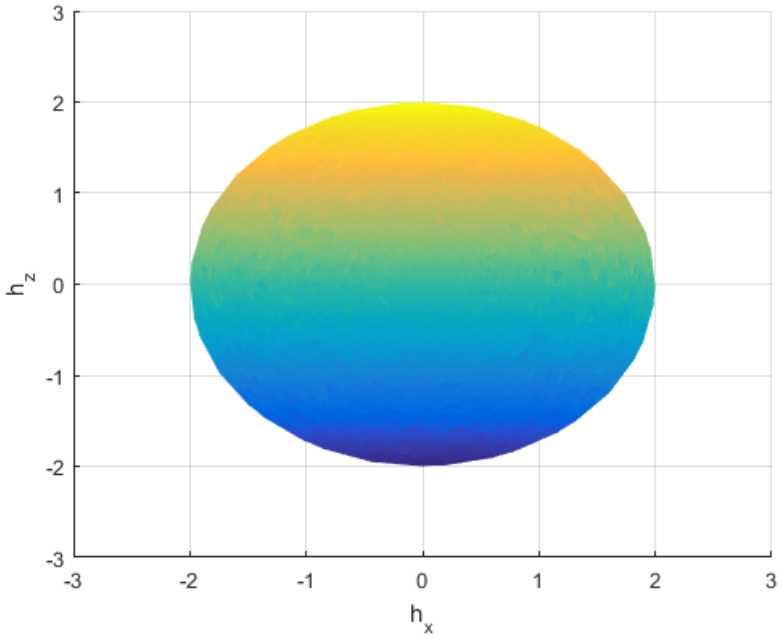

Figure B.3: Parallel Envelope X-Z Axis

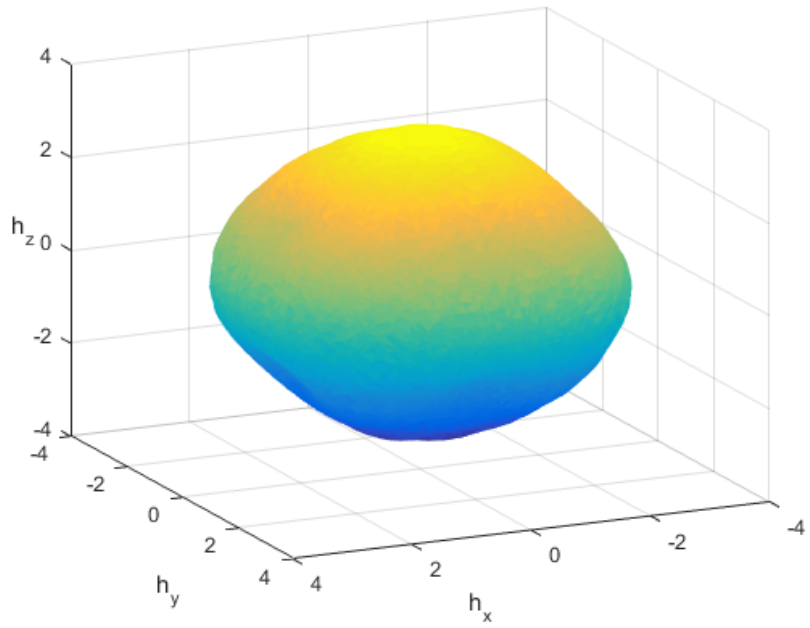

Figure B.4: Pyramid Envelope Full Axis

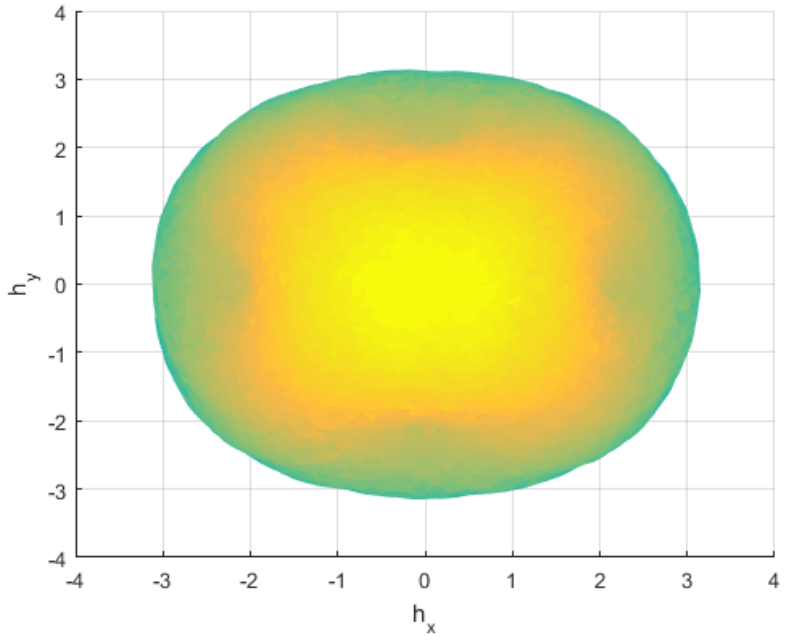

Figure B.5: Pyramid Envelope X-Y Axis

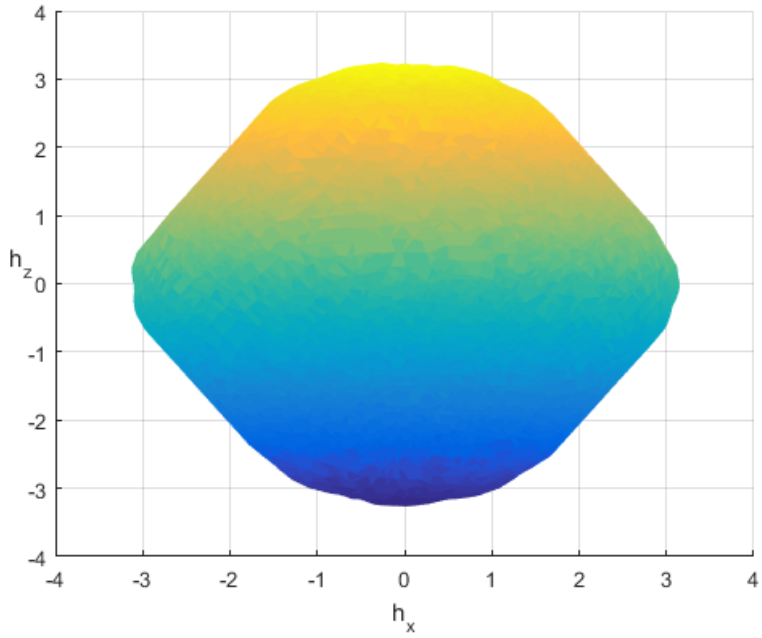

Figure B.6: Pyramid Envelope X-Z Axis

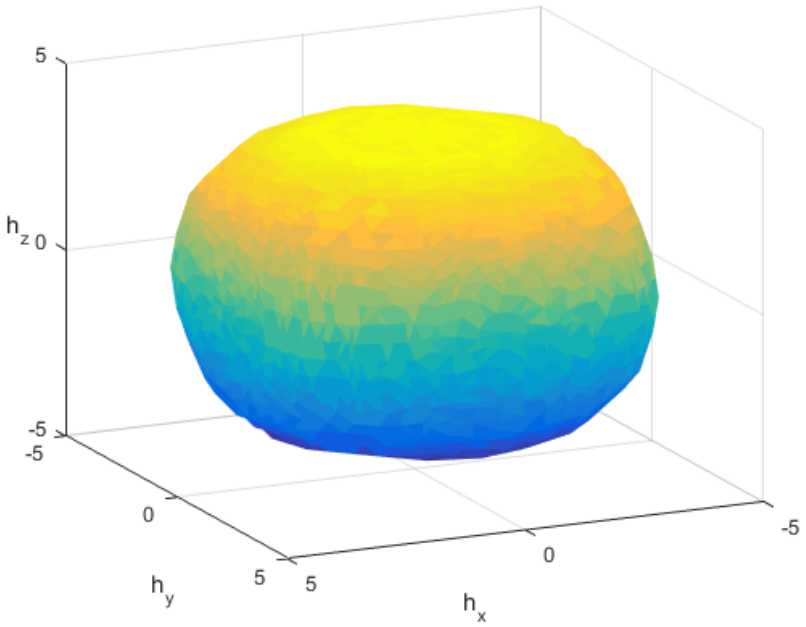

Figure B.7: Cube Envelope Full Axis

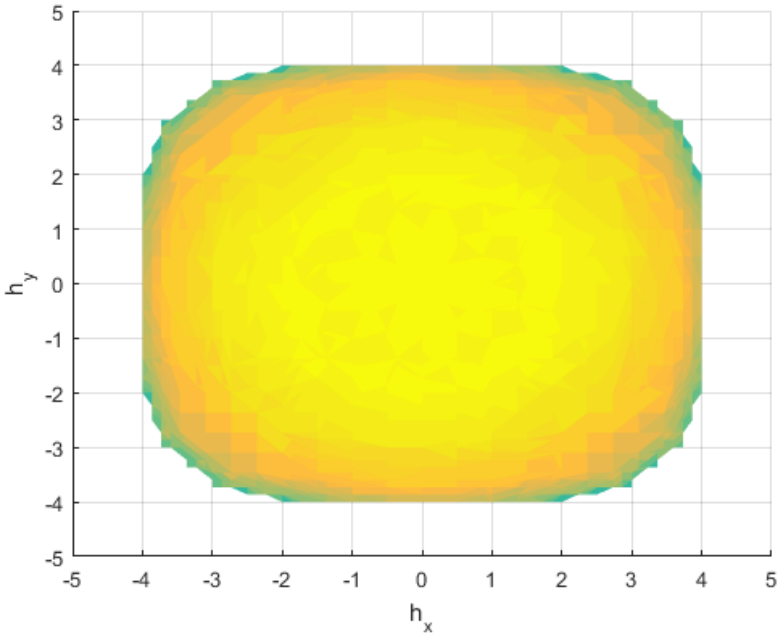

Figure B.8: Cube Envelope X-Y Axis

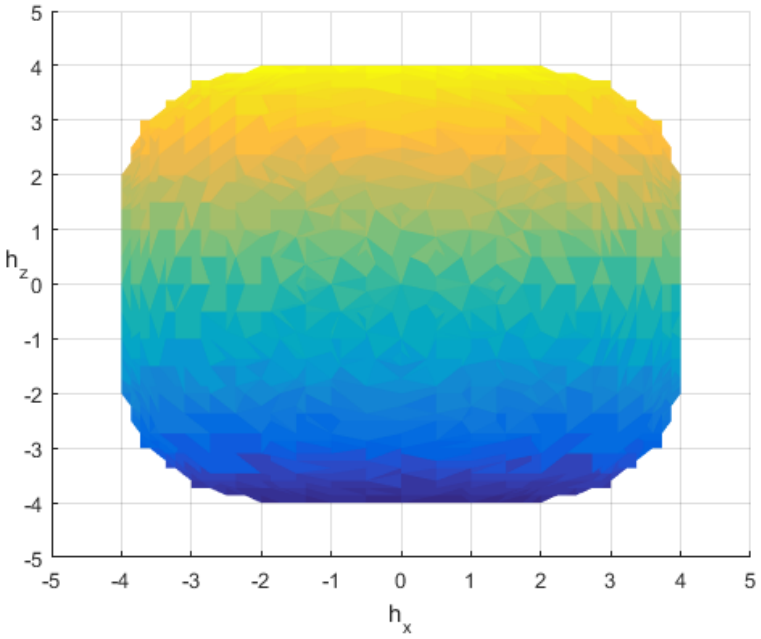

Figure B.9: Cube Envelope X-Z Axis

APPENDIX C

Simulation

The steering law for this thesis will be provided by Satellite Research Center. Instead of the standard angles for the control the SRC steering law used quaternions. The transformation from angles to quaternions is displayed in [10]. The desired torque input made of quaternions are as follows.

$$\boldsymbol{\tau}_{desired} = \mathbf{K}\left[\boldsymbol{\epsilon}_e^T \ \boldsymbol{\omega}_s^T\right]^T \tag{C.1}$$

Where $\mathbf{K}$ is obtain using model predicting control strategy. It is a 3×6 matrix with the prediction horizon of 12, control horizon of 1 and sampling time of 1 second. The value of $\mathbf{K}$ is

$$\mathbf{K} = \begin{bmatrix} -65.1479 & 0 & 0 & -276.426 & 0 & 0 \\ 0 & -54.3091 & 0 & 0 & -230.436 & 0 \\ 0 & 0 & -65.1469 & 0 & 0 & -276.426 \end{bmatrix} \tag{C.2}$$

$\boldsymbol{\epsilon}_e$ is the 1×3 error matrix of the satellites coordinate system to the target system and $\boldsymbol{\omega}_s$ is the angular velocity of the satellite which comes from the attitude determination system on board the satellite, this also is a 1×3 matrix.

The goal for the steering law is to drive the desired torque to zero. When it is zero the satellite is pointing exactly on target.

During the simulation the system experience a disturbance of $1mNm$ every second.

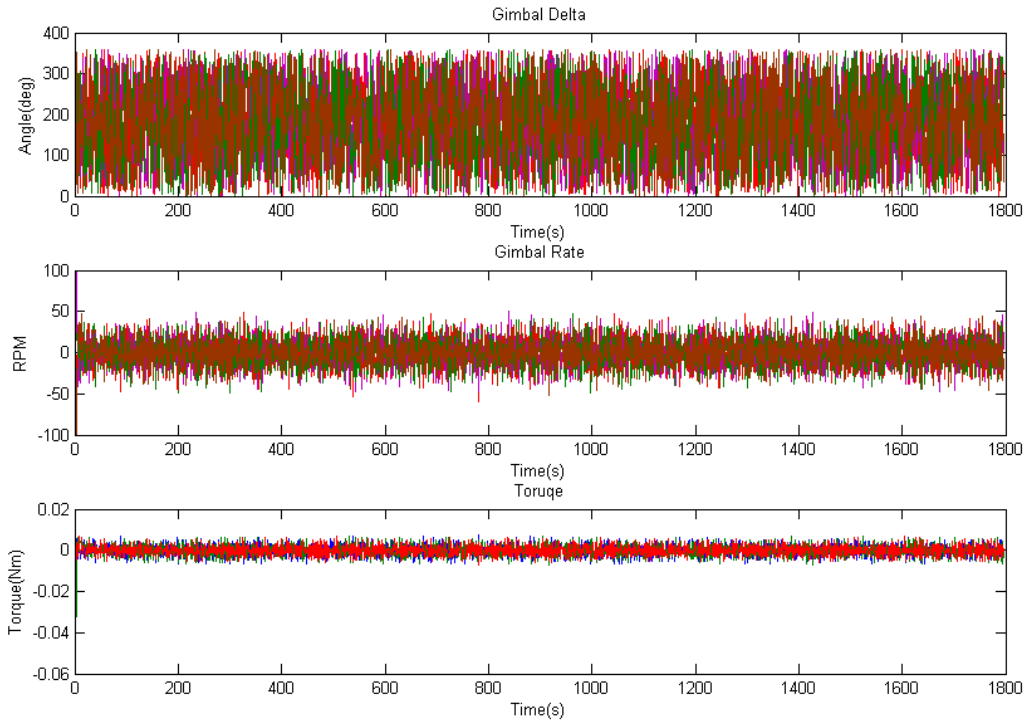

Figure C.1: Combined display of the gimbal angle, gimbal rate and torque

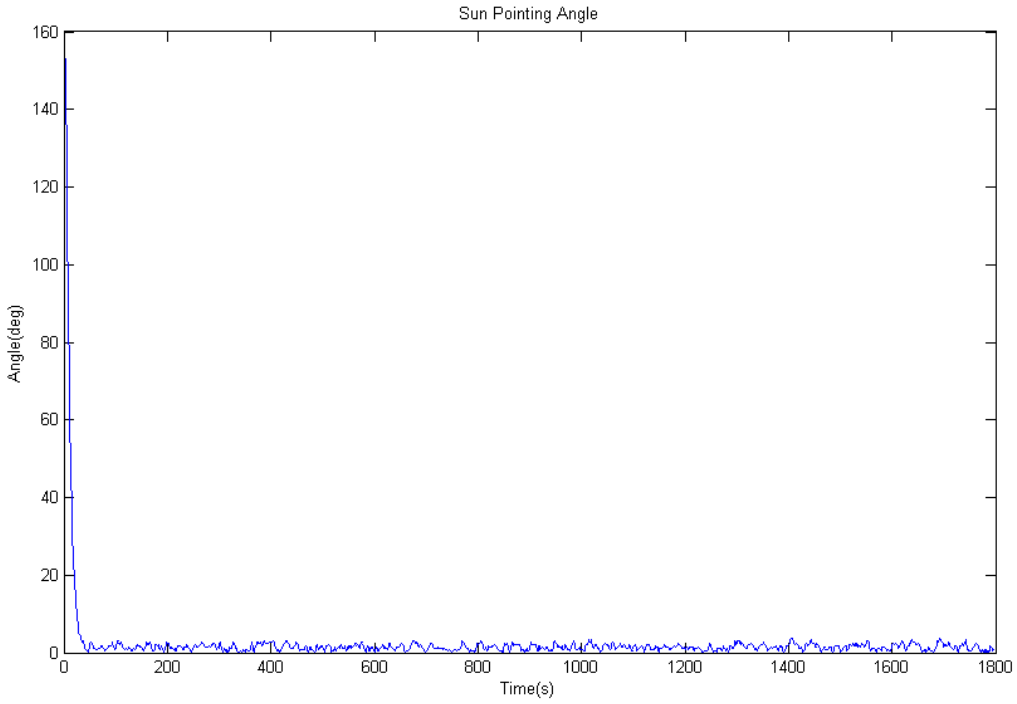

Figure C.2: Sun Pointing Error

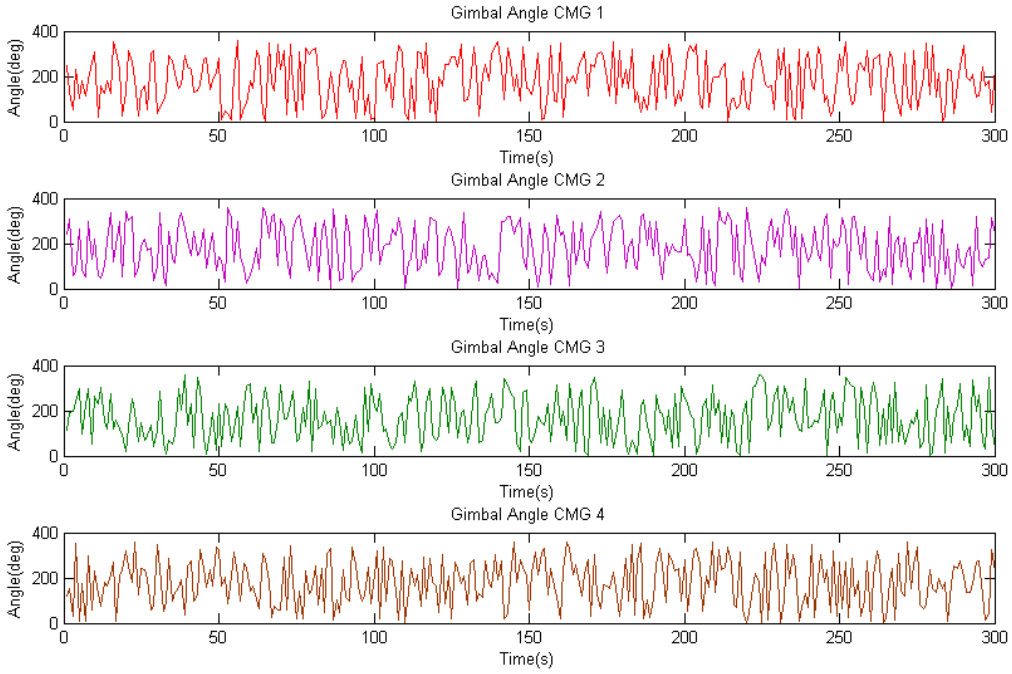

Figure C.3: Displaying each of the gimbal Angle

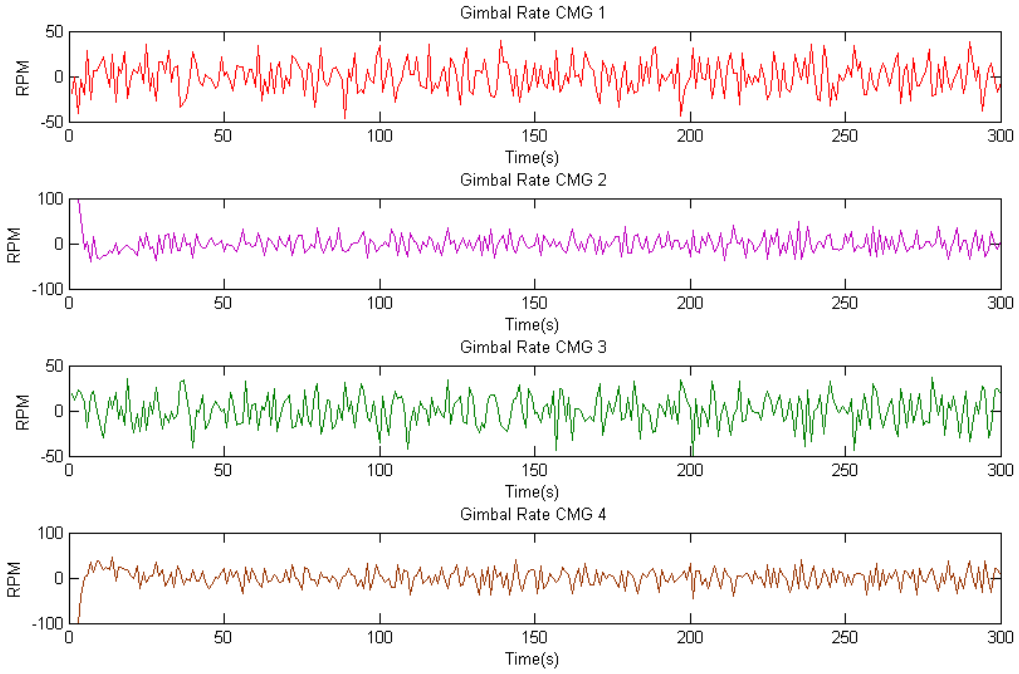

Figure C.4: Displaying each of the gimbal rate

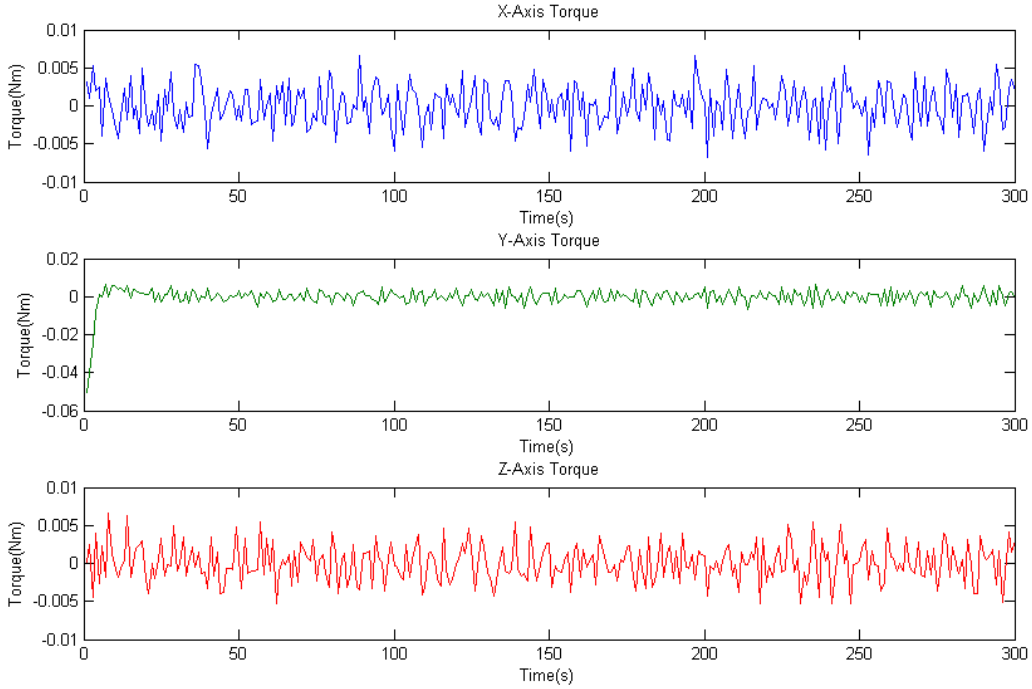

Figure C.5: Displaying each of the torque

Appendix D

Datasheets

- Brushless Flat DC-Micromotors
  The motor that rotates the flywheel
- Brushless DC-Servomotors
  The motor that rotates the reaction wheel, gimbal motor
- Motion Controller
  Drive electronics for the gimbal motor
- Encoder
  The encoder fitted on the gimbal motor
- Slip Ring
  Rotation to stationary connector

Brushless Flat DC-Micromotors 3,7 mNm

with integrated Speed Controller

Series 2610 ... B SC

		2610 T		006 B	012 B	SC
1	Nominal voltage	U_N		6	12	Volt
2	Terminal resistance, phase-phase	R		7,0	28,2	Ω
3	Output power [1]	$P_{2\ max.}$		1,92	1,91	W
4	Efficiency	$\eta_{max.}$		78	78	%
5	No-load speed	n_o		6 200	6 200	min^{-1}
6	No-load current	I_o		0,012	0,006	A
7	Stall torque	M_H		7,73	7,68	mNm
8	Friction torque, static	C_o		0,025	0,025	mNm
9	Friction torque, dynamic	C_v		$1,35 \cdot 10^{-5}$	$1,35 \cdot 10^{-5}$	mNm/min^{-1}
10	Speed constant	k_n		1 055	528	min^{-1}/V
11	Back-EMF constant	k_E		0,948	1,895	mV/min^{-1}
12	Torque constant	k_M		9,05	18,1	mNm/A
13	Current constant	k_I		0,111	0,055	A/mNm
14	Slope of n-M curve	$\Delta n/\Delta M$		816	822	min^{-1}/mNm
15	Terminal inductance, phase-phase	L		480	1 940	µH
16	Mechanical time constant	τ_m		69	70	ms
17	Rotor inertia	J		8,1	8,1	gcm^2
18	Angular acceleration	$\alpha_{max.}$		9,5	9,5	$\cdot 10^3 rad/s^2$
19	Thermal resistance	R_{th1} / R_{th2}	33 / 27			K/W
20	Thermal time constant	τ_{w1} / τ_{w2}	20 / 230			s
21	Operating temperature range		-25 ... +80			°C
22	Shaft bearings		ball bearing, preloaded			
23	Shaft load max.:					
	– radial at 3 000/7 000 min^{-1} (3 mm from mounting flange)		4,0 / 3,5			N
	– axial at 3 000/7 000 min^{-1} (push-on only)		3,5 / 3,4			N
	– axial at standstill (push-on only)		17,5			N
24	Shaft play:					
	– radial	≤	0,015			mm
	– axial	=	0			mm
25	Housing material		plastic			
26	Weight		20,1			g
27	Direction of rotation		electronically reversible			
28	Number of pole pairs		2			
Recommended values - mathematically independent of each other						
29	Speed up to	$n_{e\ max.}$		7 000	7 000	min^{-1}
30	Torque up to [1] [2]	$M_{e\ max.}$		3,14 / 3,72	3,13 / 3,70	mNm
31	Current up to [1] [2]	$I_{e\ max.}$		0,40 / 0,47	0,20 / 0,24	A

[1] at 5 000 min^{-1}

[2] thermal resistance R_{th2} not reduced / thermal resistance R_{th2} by 55% reduced

Note:

The diagram indicates the recommended speed in relation to the available torque at the output shaft for a given ambient temperature of 22°C.

The diagram shows the motor in a completely insulated as well as thermally coupled condition ($R_{th\ 2}$ 55% reduced).

The area of the curve is defined by the maximum allowable supply voltage of the integrated speed controller as well as the control performance characteristics.

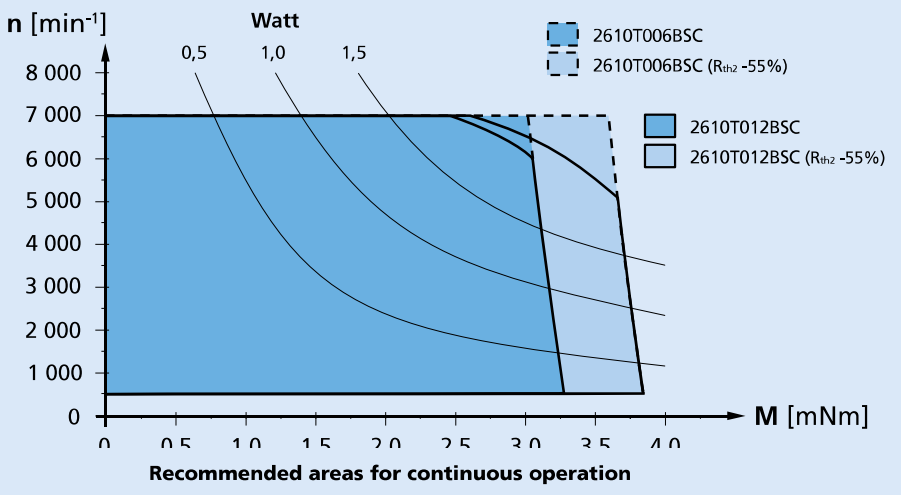

For notes on technical data and lifetime performance refer to "Technical Information".

Edition 2016

www.faulhaber.com

2610 T ... B SC

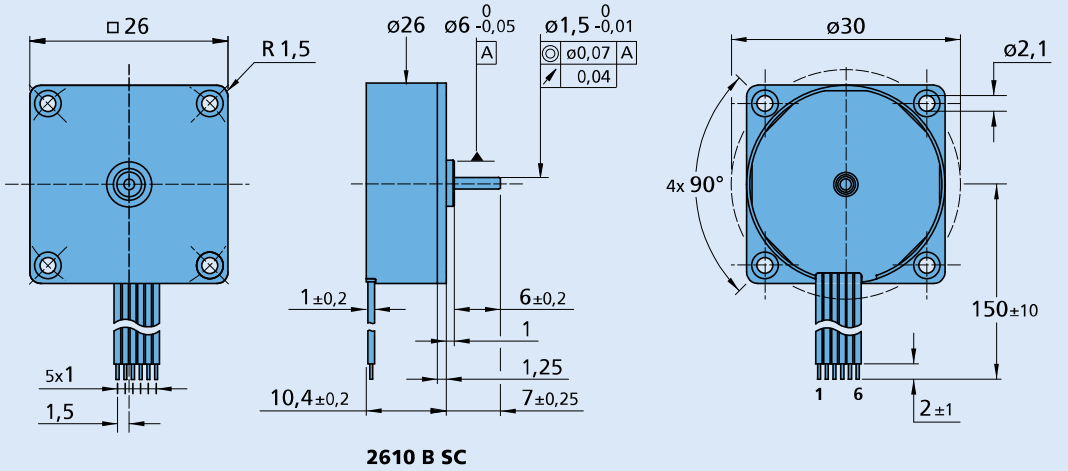

2610 B SC

Cable
Jacket Material: PVC
8 conductors, AWG 28
grid 1,0 mm
wires tinned

Note:
Hallsensors digital

Connection

No.	Function
1	U_P
2	U_{mot}
3	GND
4	U_{nsoll}
5	DIR
6	FG

Speed Controller			
PWM switching frequency	f_{PWM}	96	kHz
Efficiency	η	95	%
Max. continuous output current [1]	I_{dauer}	0,8	A
Max. peak output current	I_{max}	1,6	A
Total standby current	I_{el}	0,020	A
Speed range:			
– standard » Hall sensors (digital)		500 ... 60 000 [2]	min^{-1}
Scanning range		500	µs

[1] at 22°C ambient temperature and max. 60°C motor temperature respectively
[2] speed depend on motor operating voltage

Connection information		
Connection 1 "U_P":	power supply electronic	U_P = 4 ... 18 V
Connection 2 "U_{mot}":	power supply electronic coil	U_{mot} = 1,7 ... 18 V
Connection 3 "GND":	ground	ground
Connection 4 "U_{nsoll}":		
– analog input	input voltage	U_{in} = 0 ... 10 V (max. Up)
	input resistance	R_{in} ≥ 8 kΩ
	set speed value	per 1 V » 1 000 min^{-1}
		U_{in} < 0,15 V » motor stops
		U_{in} > 0,3 V » motor starts
Connection 5 "DIR":		
– digital input	direction of rotation	to ground or level < 0,5 V » counterclockwise
		open or level > 3 V » clockwise (max. Up)
	input resistance	R_{in} ≥ 10 kΩ
Connection 6 "FG":		with max. U_P » I_{max} = 15 mA; open collector with 22 kΩ pull-up resistor
– digital output	frequency output	6 lines per revolution

Features

In this variant, the brushless DC-Micromotors have an integrated Speed Controller. The motor is commutated using Hall sensors integrated into the motor. Speed control is via a PI regulator. The Speed Controller has a current limiting device which limits the maximum motor current if the thermal load is too high. Twice the continuous current is possible over a short time.

Using the **"FAULHABER Motion Manager"** software, the customer can modify the Speed Controller to special conditions of use.

The following parameters can be changed: current limit and regulator parameters.

Full product description

- Examples:
  2610T006B SC
  2610T012B SC

Option

- connector variants (Option no. 4257)
  AWG 28 / PVC ribbon cable with connector Picoblade

Brushless DC-Servomotors

4 Pole Technology

18 mNm

23 W

Series 2232 ... BX4

Values at 22°C and nominal voltage		2232 S	012 BX4	024 BX4	
1	Nominal voltage	U_N	12	24	V
2	Terminal resistance, phase-phase	R	3,5	12,5	Ω
3	Efficiency, max.	$\eta_{max.}$	74	74	%
4	No-load speed	n_0	6 700	7 100	min^{-1}
5	No-load current, typ. (with shaft ø 3 mm)	I_0	0,072	0,039	A
6	Stall torque	M_H	58,7	61,7	mNm
7	Friction torque, static	C_0	0,46	0,46	mNm
8	Friction torque, dynamic	C_V	$1{,}1 \cdot 10^{-4}$	$1{,}1 \cdot 10^{-4}$	mNm/min^{-1}
9	Speed constant	k_n	562	295	min^{-1}/V
10	Back-EMF constant	k_E	1,78	3,393	mV/min^{-1}
11	Torque constant	k_M	17	32,4	mNm/A
12	Current constant	k_I	0,059	0,031	A/mNm
13	Slope of n-M curve	$\Delta n/\Delta M$	114	114	min^{-1}/mNm
14	Terminal inductance, phase-phase	L	115	410	µH
15	Mechanical time constant	τ_m	6,1	6,1	ms
16	Rotor inertia	J	5,1	5,1	gcm^2
17	Angular acceleration	$\alpha_{max.}$	115	121	$\cdot 10^3 rad/s^2$
18	Thermal resistance	R_{th1} / R_{th2}	3,9 / 18,8		K/W
19	Thermal time constant	τ_{w1} / τ_{w2}	7,9 / 520		s
20	Operating temperature range:				
	– motor		-40 ... +100		°C
	– winding, max. permissible		+125		°C
21	Shaft bearings		ball bearings, preloaded		
22	Shaft load max.:				
	– with shaft diameter		3		mm
	– radial at 3 000 min^{-1} (5 mm from mounting flange)		20		N
	– axial at 3 000 min^{-1} (push only)		2		N
	– axial at standstill (push only)		20		N
23	Shaft play:				
	– radial	≤	0,015		mm
	– axial	=	0		mm
24	Housing material		stainless steel		
25	Mass		65		g
26	Direction of rotation		electronically reversible		
27	Speed up to	$n_{max.}$	29 000		min^{-1}
28	Number of pole pairs		2		
29	Hall sensors		digital		
30	Magnet material		NdFeB		
Rated values for continuous operation					
31	Rated torque	M_N	14,7	14,6	mNm
32	Rated current (thermal limit)	I_N	1	0,54	A
33	Rated speed	n_N	4 450	4 840	min^{-1}

Note: Rated values are calculated with nominal voltage and at a 22°C ambient temperature. The R_{th2} value has been reduced by 25%.

Note:

The diagram indicates the recommended speed in relation to the available torque at the output shaft for a given ambient temperature of 22°C.

The diagram shows the motor in a completely insulated as well as thermally coupled condition (R_{th2} 50% reduced).

The nominal voltage (U_N) curve shows the operating point at nominal voltage in the insulated and thermally coupled condition. Any points of operation above the curve at nominal voltage will require a higher operating voltage. Any points below the nominal voltage curve will require less voltage.

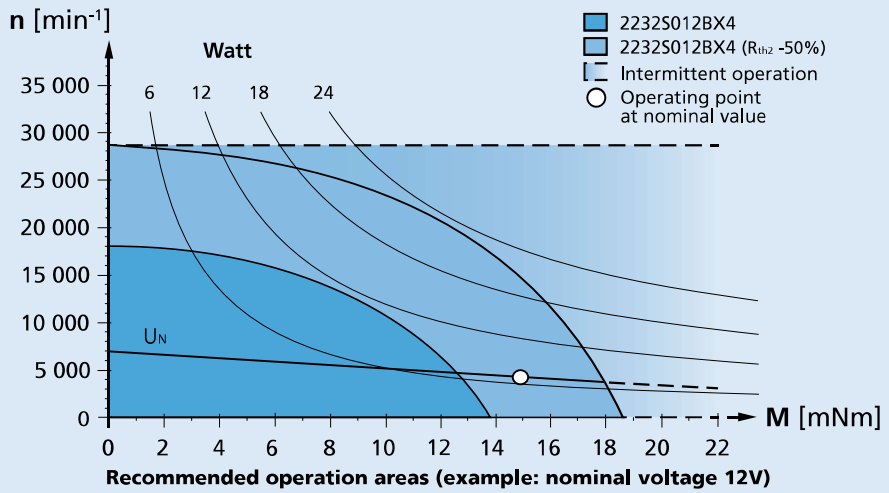

Recommended operation areas (example: nominal voltage 12V)

For notes on technical data and lifetime performance refer to "Technical Information".

Edition 2016

www.faulhaber.com

Dimensional drawing

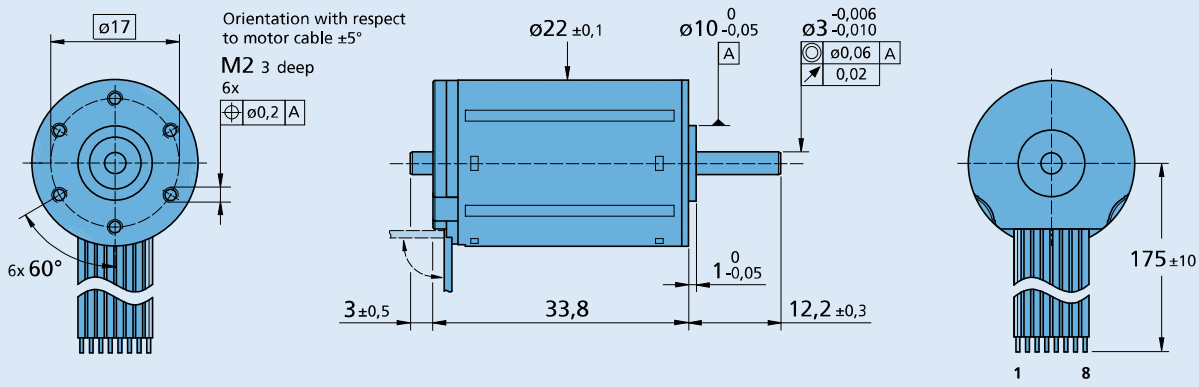

2232 S ... BX4

Option, cable and connection information

Example product designation: **2232S012BX4-3692**

Option	Type	Description
3830	Connector	AWG 26 / PVC ribbon cable with connector MOLEX Microfit 3.0, 43025-0800, recommended mating connector 43020-0800
4935	Single wires	Motor with single wires (PTFE), length 175 mm, AWG26
X4935	Single wires	Motor with single wires (PTFE), length 300 mm, AWG26
Y4935	Single wires	Motor with single wires (PTFE), length 600 mm, AWG26
4747	Temperature range	Up to 150°C, winding max. 150°C, with single wires (PTFE), length 175 mm, AWG26
X4747	Temperature range	Up to 150°C, winding max. 150°C, with single wires (PTFE), length 300 mm, AWG26
Y4747	Temperature range	Up to 150°C, winding max. 150°C, with single wires (PTFE), length 600 mm, AWG26
Y158	Shaft end	Motor without second shaft end
3692	Controller combination	Analog Hall sensors for combination with Motion Controller MCBL

Connection standard

No.	Function	Option: 4935/4747 Function	Colour
1	Phase C	Phase C	yellow
2	Phase B	Phase B	orange
3	Phase A	Phase A	brown
4	GND	GND	black
5	U_{DD} (+5V)	U_{DD} (+5V)	red
6	Hall sensor C	Hall sensor C	grey
7	Hall sensor B	Hall sensor B	blue
8	Hall sensor A	Hall sensor A	green

Standard cable

Insulation: PVC
8 conductors, AWG 26
pitch 1,27 mm, wires tinned

Product Combination

Precision Gearheads / Lead Screws	Encoders	Drive Electronics	Cables / Accessories
22F 22/7 26A BS22-1.5	IE3-1024 IE3-1024 L AES-4096	SC 1801 SC 2402 SC 2804 SC 5004 SC 5008 MCBL 3002 MCBL 3003 MCBL 3006	6501.00085 Motor adapter for MCBL 3002 S / SC 1801 (motor with connector 3830) 6501.00086 Motor adapter for MCBL 3006 S / SC 2804 and 5008 (motor with connector 3830) 6501.00141 Extension cable, motor with connector 3830, 8 single wires, length 300 mm for combination with SC and MC 6501.00142 Extension cable, motor with connector 3830, 8 single wires, length 1000 mm for combination with SC and MC

Motion Controller

V2.5, 4-Quadrant PWM
with RS232 or CAN interface

For combination with:
Brushless DC-Servomotors
with absolute encoder

Series MCBL 3002 AES

		MCBL 3002 P AES	MCBL 3002 F AES	MCBL 3002 S AES	
Power supply	U_B	5 ... 30	5 ... 30	5 ... 30	V DC
PWM switching frequency	f_{PWM}	78,12	78,12	78,12	kHz
Efficiency	η	95	95	95	%
Max. continuous output current [1]	I_{dauer}	2	2	2	A
Max. peak output current	I_{max}	3	3	3	A
Total standby current	I_{el}	0,04	0,04	0,04	A
Speed range		5 ... 30 000	5 ... 30 000	5 ... 30 000	min^{-1}
Scanning rate	N	100	100	100	µs
Encoder resolution with AES encoder		≤ 4 096	≤ 4 096	≤ 4 096	inc./rev.
Resolution with external encoder		≤ 65 535	≤ 65 535	≤ 65 535	inc./rev.
Input/output (partially free configurable)		3	3	3	
Program memory: [2]					
– memory size		3,3	3,3	3,3	kWord
– Number of instructions		ca. 1 000	ca. 1 000	ca. 1 000	instructions
Operating temperature range		– 25 ... + 85	– 25 ... + 85	– 25 ... + 85	°C
Weight		7	13	16	g

[1] at 22°C ambient temperature
[2] Only for version with serial interface

Connection information					
Connection communication:					
Interface			RS232	CAN	
Communication profile			FAULHABER - ASCII	CANopen	
Max. transfer speed rate RS232			115 200		baud
Max. transfer speed rate CAN				1	Mbit/s
Connection 3 "AGND":					
– analog ground			analog GND		
– digital input	external encoder		channel B		
		R_{In}	10		kΩ
		f	≤ 400		kHz
Connection 4 "Fault":					
– digital input		R_{In}	100		kΩ
– digital output (open collector)		U	≤ U_B		V
		I	≤ 30		mA
		clear	switched to GND		
		set	high-impedance		
	fault output	no error	switched to GND		
		error	high-impedance		
	signal output	f	≤ 2		kHz
		resolution	1...32		inc./rev.
Connection 5 "AnIn":			"AGND" as GND		
– analog input	set speed value	U_{In}	± 10		V
– digital input	PWM set speed value	f	100 ... 2 000		Hz
		T	50% ≙ 0 min^{-1}		
	external encoder		channel A		
		f	≤ 400		kHz
	step frequency input	f	≤ 400		kHz
		R_{In}	5		kΩ
Connection 6 "U_B":		U_B	5 ... 30		V DC
Connection 7 "GND":			ground		
Connection 8 "3. In":					
– digital input		R_{In}	22		kΩ
– electronic supply voltage		U_{EL}	5 ... 30		V DC

Connection information

Connection 9-11 „DATA, $\overline{CS}$, CLK ":				
	DATA	U_{In}	≤ 5	V
	$\overline{CS}$	U_{Out}	0 ... 5	V
	CLK	U_{Out}	0 ... 5	
Connection 12 "U_{CC}":				
Output voltage for external use [1]		U_{Out}	5	V
Load current		I_{Out}	≤ 60	mA
Connection 13 "SGND":				
Signal GND			Signal ground	
Connection 14-16 „Motor A, B, C":				
Motor connection	Motor A		Phase A	
	Motor B		Phase B	
	Motor C		Phase C	
		U_{Out}	0 … U_B	V DC
PWM switching frequency		f_{PWM}	78,12	kHz

[1] E.g. encoder

The signal level (PLC or TTL) of the digital inputs can be set over the interface (see operating instruction manual).
Standard (PLC): Low 0...4,5V / High 12,5V... U_B, TTL: Low 0...0,5V / High 2,5V... U_B

Options

- Separate power supply (Option no.: 3085)

Full product description

- Example:
  MCBL 3002 S AES RS (RS232)
  MCBL 3002 F AES CF (CANopen with FAULHABER CAN)
  MCBL 3002 P AES CO (CANopen CiA)

Accessories

		Motor Type	Part No. for MCBL 3002 S AES, F AES
Programming adapter	**RS232/CAN**	BL	**6501.00121**

Dimensional drawing and connection information MCBL 3002 S AES

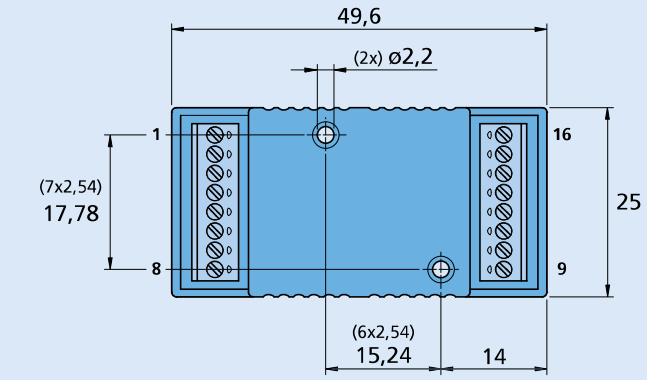

MCBL 3002 S AES

Supply connection

No.	Function
1	TxD / CAN_H
2	RxD / CAN_L
3	AGND
4	Fault
5	AnIn
6	U_B
7	GND
8	3. In

Motor connection

No.	Function
9	Sensor A / DATA
10	Sensor B / $\overline{CS}$
11	Sensor C / CLK
12	UCC
13	SGND
14	Motor A
15	Motor B
16	Motor C

Dimensional drawing and connection information MCBL 3002 P AES

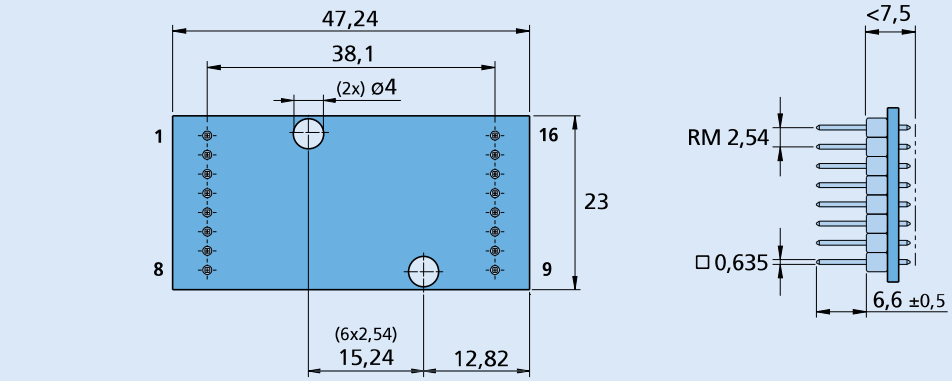

MCBL 3002 P AES

Supply connection

No.	Function
1	TxD / CAN_H
2	RxD / CAN_L
3	AGND
4	Fault
5	AnIn
6	U_B
7	GND
8	3. In

Motor connection

No.	Function
9	Sensor A / DATA
10	Sensor B / $\overline{CS}$
11	Sensor C / CLK
12	UCC
13	SGND
14	Motor A
15	Motor B
16	Motor C

Dimensional drawing and connection information MCBL 3002 F AES

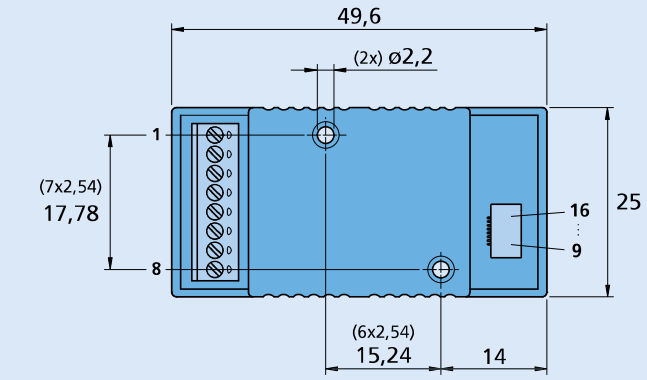

MCBL 3002 F AES

Connector Information
LIF-Connector 8-pole

Supply connection

No.	Function
1	TxD / CAN_H
2	RxD / CAN_L
3	AGND
4	Fault
5	AnIn
6	U_B
7	GND
8	3. In

Motor connection

No.	Function
9	Sensor A / DATA
10	Sensor B / $\overline{CS}$
11	Sensor C / CLK
12	UCC
13	SGND
14	Motor A
15	Motor B
16	Motor C

Encoders

magnetic absolute Encoder, SSI Interface,
4096 lines per revolution

For combination with
Brushless DC-Motors

Series AES-4096

		AES-4096	
Lines per revolution	N	4 096	
Resolution		12 Bit	
Signal output		Synchronous Serial Interface (SSI)	
Supply voltage	U_{DD}	4,5 ... 5,5	V
Current consumption, typical [1]	I_{DD}	typ. 16, max. 23	mA
Output current, max. (DATA) [2]		4	mA
Clock Frequency, max. (CLK)		2	MHz
Input low level (CLK)		0 ... 0,8	V
Input high level (CLK)		2 ... U_{DD}	V
Setup time after power on, max.	t_{setup}	4	ms
Timeout	$t_{timeout}$	16	µs
Inertia of code disc	J	0,08	gcm²
Operating temperature range		-40 ... +100	°C

[1] U_{DD} = 5 V: with unloaded outputs
[2] U_{DD} = 5 V: low logic level < 0,4 V, high logic level > 4,6 V: CMOS- and TTL compatible

For combination with Motor	
Dimensional drawing A	**<L1 [mm]**
2232 ... BX4	50,2
2232 ... BX4 S	50,2
2250 ... BX4	68,2
2250 ... BX4 S	68,2
Dimensional drawing B	**<L1 [mm]**
3242 ... BX4	60,0
3268 ... BX4	86,0

Characteristics

The absolute encoder in combination with the Faulhaber motors is ideal for commutation, speed and position control. It can also be used to create a sinusoidal commutation signal.

In the AES version, absolute position information is provided with a resolution of up to 4096 steps per revolution at the signal outputs and communicated via a serial (SSI) interface. Absolute means, that each shaft position is assigned to a unique angular value within one revolution. This value is already available directly after power-on.

The advantages are a reduced torque ripple, a higher efficiency, and reduced electrical noise generation. When using sinusodial commutation.

Motor and encoder are connected via a common ribbon cable.

Circuit diagram / Output signals

Output circuit

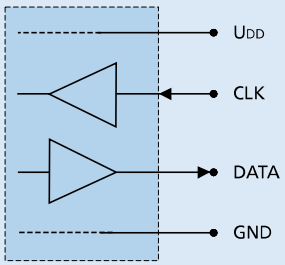

Interface signals (SSI)

Angle position values are ascending for clockwise rotation.
Clockwise rotation as seen from the shaft end.

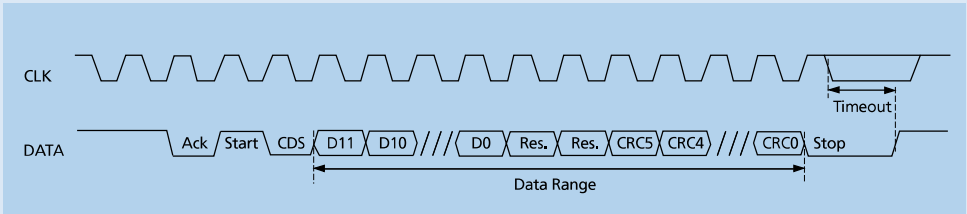

Connector information / Variants

No.	Function
1	Phase C
2	Phase B
3	Phase A
4	GND
5	U_{DD}
6	CLK
7	N.C.
8	DATA

Connection Encoder and Motor

Option

- Connector variants (Option no.: 3830)
  AWG 26 / PVC ribbon cable with connector MOLEX Microfit 3.0, 43025-0800, recommended mating connector 43020-0800

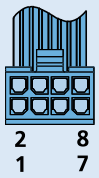

Caution:
Incorrect lead connection will damage the motor electronics!

Full product description

- Example:
  2232S012BX4 AES-4096
  3242G024BX4 AES-4096

Dimensional drawing A

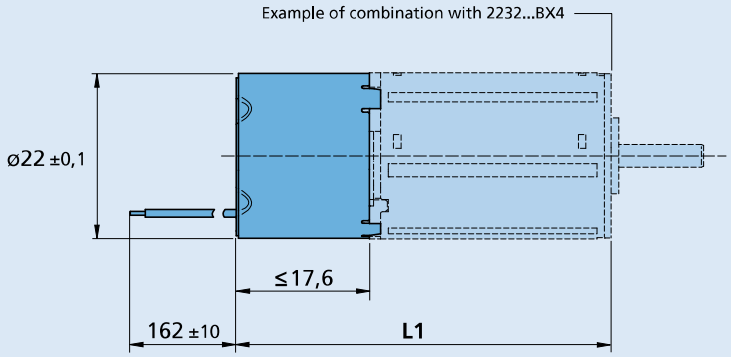

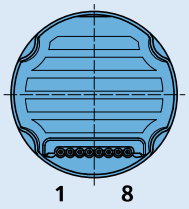

Cable
PVC-ribbon cable
8-AWG 26, 1,27 mm

AES-4096

Dimensional drawing B

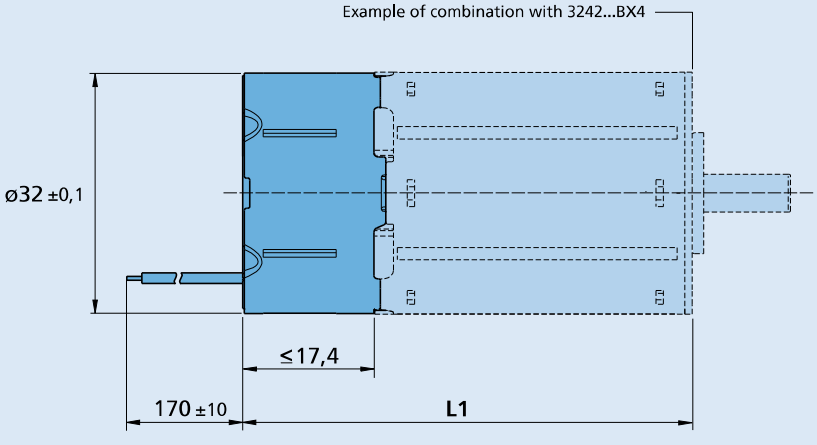

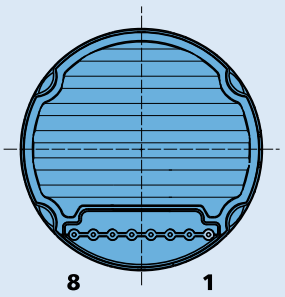

Cable
PVC-ribbon cable
8-AWG 24, 2,54 mm

AES-4096

Separate Slip Ring

Main Application

- Electrical test equipment
- Manufacturing and process control equipment
- Indexing tables
- CCTV pan / tilt camera mounts
- Robotics, rotary sensors, urgent illumination equipment
- Exhibit / display equipment
- Medical equipment
- Aviation, military, instrument
- Mini-type wire-rolling machine
- Custom Machinery
- OEM Machinery

Contact us to discuss your special needs

LPS-06A-Rotor
LPS-06B- Stator
Separate Slip Ring

Description

This unit can be used in any electromechanical system that requires unrestrained, continuous rotation while transferring power or data from a stationary to a rotating structure.

It is also called a rotary electrical interface, commutator, collector, swivel or an electrical rotary joint. It can improve electromechanically capability, simplify system design, eliminate possible damage while rotation. It's the key apparatus of various precision rotary worktable, electric test instrument, manufacture and process control instrument.

The LPS-06 separate slip ring is a standard, off-the-shelf unit that uses gold contacts at the rotary interface. Color-coded lead wires are used on both the stator and rotor for simplifying electrical connections.

Using a 90° V-groove ring design for each ring, the LPS-06 provides smoother running, lower torque and lower electrical noise than competitive slip rings.

Features

- 6 circuits models
- Speed up to 300 rpm continuous
- Gold-Gold contacts
- 250mm standard lead length
- Compatible with data bus protocols
- Sealed units are available
- Flexible, color-coded, silver-plated, Teflon® UL lead wires
- Precision ball bearings meet or exceed life requirements for most commercial applications

Advantage

- Low torque minimizes system torque budget
- Compact design to fit in the most demanding space.
- Smooth running
- Low electrical noise
- Quick shipment per your urgent requirement
- 360° continuous rotation
- High bandwidth transfer capability

Separate Slip Ring

Specifications	
Operating Speed	0-100 rpm
Number of Circuits	6
Voltage	240 VAC/DC
Current Rating	1-3A
Temperature Range	-20℃ to +60℃
Working Humidity	60%RH or higher
Contact Material	Gold to Gold
Lead Size	28 # silver plated copper Teflon® UL
Lead Length	Standard 250 mm (9.843inch)
Dielectric Strength	≥500 VAC @50Hz, between each circuit
Body Material	Precious metal
Insulation Resistance	1000 MΩ @ 500 VDC
Electrcial Noise	1 mΩ Min

Separate Slip Ring		
# of Circuits	OD (mm)	Part No
6	Φ14.73	LPS-06

Lead Wire Color Codes	
Ring# Color Code	Ring# Color Code
#1 BLK	#4 ORG
#2 BRN	#5 YEL
#3 RED	#6 GRN

- The operating life of the unit depends upon temperature, rotation speed and environment.
- The operating life ≥50,000,000 runs ref.

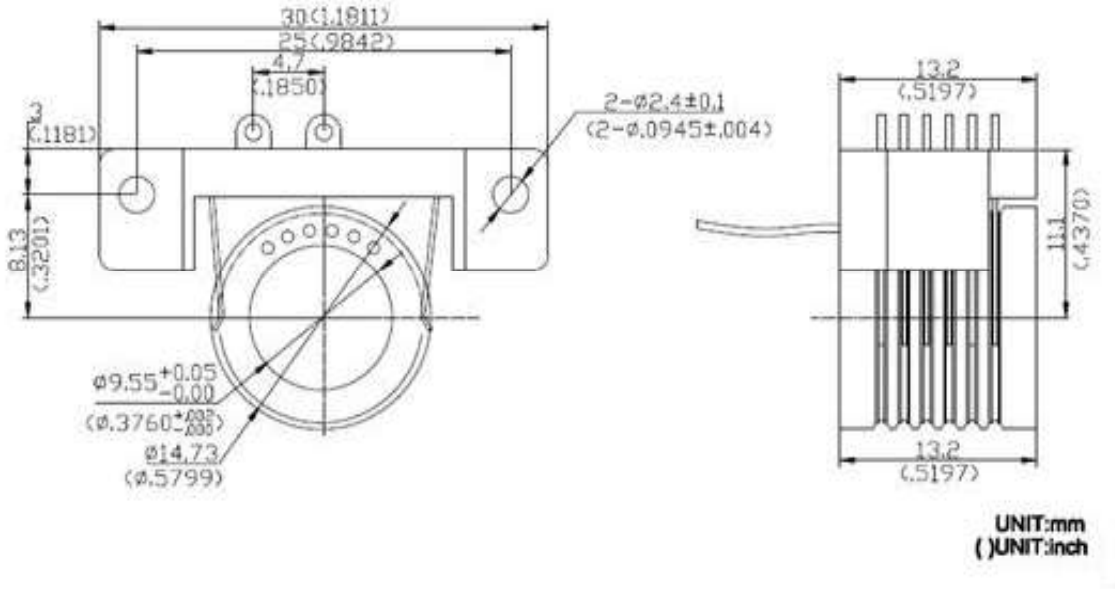

JINPAT Electronics Co.,Ltd
Email: sales@slipring.cn
www.slipring.cn
Tel: +86 755 8204 2235

References

[1] V. Ronny and S. Doug, "Comparison of control moment gyros and reaction wheels for small earth-observing satellites." 26th Annual AIAA/USU Conference on small satellite, 7 2012.

[2] R. Berner, "Control moment gyro actuator for small satellite application," Master's thesis, University of Stellenbosch, 4 2005.

[3] D. Steyn, "Variable speed scissored pair dual gimbal control moment gyro for nano-satellites," Master's thesis, Stellenbosch University, 4 2013.

[4] B. Wie, "Singularity analysis and visualization for single-gimbal control moment gyro systems," *JOURNAL OF GUIDANCE, CONTROL & DYNAMICS*, vol. 27, pp. 271–282, 3 2004. An optional note.

[5] V. J. Lappas, *A Control Moment Gyro (CMG) Based Attitude Control System (ACS) For Agile Small Satellites*. PhD thesis, University of Surrey, 2002.

[6] T. X. Y. CALVIN, "Design of a control moment gyroscope for small satellites," Master's thesis, Nanyang Technological University, 4 2013.

[7] F. Leve, B. Hamilton, and M. Peck, *Spacecraft Momentum Control System*, vol. 34 of *1*. Springer, 1 ed., Jan. 2015.

[8] W. Chubb and S. M. Seltzer, "Skylab attitude and pointing control system," Tech. Rep. 1, National Aeronautics and Space Administration, Feb. 1972.

[9] G. Charles, S. Raymond, and D. Scott, "Space station control moment gyroscope lessons learned," vol. 1, pp. 161–176, May 2010.

[10] L. Markley and J. Crassidis, *Fundamentals of Spacecraft Attitude Determination and Control*, vol. 33 of *1*. Springer, 1 ed., Jan. 2014.

[11] J. Wright, E. Swenson, and F. Keve, "Hardware testing of hybrid steering logic for single-gimbal control moment gyroscopes," vol. 1, August 2012.

[12] InnovativeSolutionsInSpace, “"http://www.http://isispace.nl/".” Online; accessed August 08, 2016.

[13] CubeSatShoppen.com, “"http://www.cubesatshop.com/index.php?page=shop.product_details&flypage=flypage.tpl&product_id=45&category_id=1&option=com_virtuemart&Itemid=66&vmcchk=1&Itemid=66".” Online; accessed April 18, 2016.

[14] C. Nordling and J. Osterman, *Physics Handbook for Science and Engineering*, vol. 1 of *1*. Studentlitteratur, 8 ed., Feb. 2006.

[15] E. J. R.Wertz, *Spacecraft Attitude Determination and Control*, vol. 73 of *1*. Kluwer Academic Publishers, 1 ed., Jan. 1978.

[16] P. Berlin, *Satellite Platform Design*, vol. 1 of *1*. LuleåUniversity of Technology, 6 ed., Feb. 2014.

[17] J. Fisher, R. Bhattacharya, and S. Vadali, “Controllability of spacecraft attitude using control moment gyroscopes,” in *AIAA Guidance, Navigation and Control Conference and Exhibit*, vol. 1 of *1*, p. 1, 8 2007.

[18] S. R. Center, “Nanyang technological university.” http://www.sarc.eee.ntu.edu.sg/Research/Projects/Pages/VELOX-II.aspx, accessed April 18, 2016.

[19] “Tillägg till physics handbook,” 10 2007. Reviderad 2012-11-02.

[20] V. Nagabhusham, “Development of control moment gyroscopes for attitude control of small satellites,” Master’s thesis, University of Florida, 4 2009.

[21] H. Yoon and P. Tsiotras, “Spacecraft line-of-sight control using a single variable-speed control moment gyro,” in *JOURNAL OF GUIDANCE, CONTROL, AND DYNAMICS*, vol. 29 of *6*, p. 1295, 11 2006.

[22] V. Lappas, P. Oosthuizen, P. Madle, L. Cowie, G. Yuksel, and D. Fertin, “Design, analysis and in-orbit performance of the bilsat-1 microsatellite twin control moment gyroscope experimental cluster,” in *AIAA Guidance, Navigation and Control Conference and Exhibit*, vol. 1 of *1*, p. 1, 8 2004.

[23] B. Wie, “2h singularity-free momentum generation with non-redundant single gimbaled control moment gyroscopes,” *IEEE Conference on Decision & Control*, vol. 27, pp. 271–282, 3 2004. An optional note.

[24] C. McChesney, “Attitude control actuators for a simulated spacecraft,” in *AIAA Guidance, Navigation and Control Conference*, vol. 1 of *1*, p. 1, 8 2011.

[25] J. Fisher, R. Bhattacharya, and S. Vadali, "Spacecraft momentum management and attitude control using a receding horizon approach," in *AIAA Guidance, Navigation and Control Conference and Exhibit*, vol. 1 of *1*, p. 1, 8 2007.

[26] V. Lappas, W. Steyn, and C. Underwood, "Attitude control for small satellite using control moment gyros," accessed June 20, 2016.

[27] Faulhaber, `http://www.faulhaber.com/en/SG/`, *Drive Systems*, 1 ed., 1 2016. We Create Motion.

[28] J. Electronics, "`"http://www.slipring.cn/products_LPS.php"`." Online; accessed April 18, 2016.

[29] MISUMI, "`"http://www.http://uk.misumi-ec.com/"`." Online; accessed October 04, 2016.

[30] D. F. Faulhaber, *Communication and Function Manual.* Faulhaber, 4 ed., 4 2015.

[31] HoneybeeRobotics, "`"http://www.honeybeerobotics.com/portfolio/microsat-control-moment-gyroscopes/"`." Online; accessed August 30, 2016.